NASA Contractor Report 3675

An Aerodynamic Analysis Computer Program and Design Notes for Low Speed Wing Flap Systems

Harry W. Carlson and Kenneth B. Walkley

NASA

NASA Contractor Report 3675

An Aerodynamic Analysis Computer Program and Design Notes for Low Speed Wing Flap Systems

Harry W. Carlson and Kenneth B. Walkley
Kentron International, Inc.
Hampton, Virginia

NASA

National Aeronautics
and Space Administration

**Scientific and Technical
Information Branch**

1983

SUMMARY

This report describes the expanded capabilities for analysis and design of low speed flap systems afforded by recent modifications of an existing computer program. The program provides for the simultaneous analysis of up to 25 pairs of leading-edge and trailing-edge flap deflection schedules. Among other new features of the program are a revised attainable thrust estimation method to provide more accurate predictions for low Mach numbers, and a choice of three options for estimation of leading-edge separation vortex flow effects.

Comparison of program results with low speed experimental data for an arrow wing supersonic cruise configuration with leading-edge and trailing-edge flaps showed good agreement over most of the range of flap deflections. Other force data comparisons and an independent study of airfoil and wing pressure distributions indicated that wind-tunnel measurements of the aerodynamic performance of twisted and cambered wings and wings with leading-edge flaps can be very sensitive to Reynolds number effects.

INTRODUCTION

The low speed aerodynamic analysis method of reference 1 provides estimates of wing performance which include the effects of attainable leading-edge thrust and vortex lift. The method was shown to be particularly useful in the subsonic analysis of vehicles designed for supersonic cruise. In reference 2, the computer program described in reference 1 was used as an aid in the design of low speed leading-edge flaps for a candidate supersonic transport configuration.

This report describes modifications and improvements to the original computer program to permit more convenient, more accurate, and more efficient treatment of simple leading and trailing-edge flap systems. In this improved program, there is provision for direct input of flap geometry. For the study of reference 2 it was necessary to make internal program modifications. In addition, the program is arranged so that, with little additional expense, solutions may be found for various combinations of leading and trailing-edge flap deflections.

Another improvement incorporated in the present computer program is a revised attainable thrust algorithm which is more accurate at the low Mach numbers sometimes encountered in wind tunnel testing. A means of estimating the distribution of leading-edge separation vortex forces has also been provided.

The applicability of the program results to the aerodynamic analysis of wings with flaps is demonstrated through correlations with experimental data. In addition, suggestions for use of the program in an iterative fashion for flap system design are given.

SYMBOLS

AR	wing aspect ratio, b^2/S
b	wing span
c	local wing chord
$\bar{c}$	mean aerodynamic chord
c_{ave}	average wing chord, S/b
c_A	section axial force coefficient
c_N	section normal force coefficient
$\Delta c_{N,v}$	section normal force coefficient increment due to the leading edge separation vortex
c_n	chord of wing section normal to local wing leading edge with maximum thickness at mid chord

$$c_n = \frac{2\eta}{sin\Lambda_L[(1+\eta)tan\Lambda_L + \eta tan\Lambda_T] + cos\Lambda_L}$$

c_R	section resultant force coefficient
c_t	theoretical section leading-edge thrust coefficient
$c_{t,F}$	theoretical section leading-edge thrust coefficient for a flat wing at 1° angle of attack
C_A	total axial force coefficient
C_N	total normal force coefficient
C_D	total drag coefficient
$C_{D,0}$	drag coefficient at zero lift for a flat wing
ΔC_D	drag coefficient due to lift, $C_D - C_{D,0}$
C_L	total lift coefficient
$C_{L,\alpha}$	total lift curve slope, per degree
C_p	pressure coefficient
$C_{p,lim}$	limiting pressure coefficient used in definition of attainable thrust
$\Delta C_{p,v}$	incremental pressure coefficient due to detached leading edge vortex

3

E, e	exponents used in $C_{p,lim}$ equation
k	arbitrary constant
m	flap deflection multiplier
M	free-stream Mach number
M_n	Mach number normal to local wing leading-edge sweep angle, $M_n = M \cos \Lambda_L$
R	free-stream Reynolds number based on $\bar{c}$
R_n	Reynolds number normal to local wing leading edge, $$R_n = R \frac{c_n}{\bar{c}} \cos \Lambda_L$$
r	wing section leading-edge radius
r^*	effective leading-edge radius for attainable thrust calculation
S	wing reference area
S_s	suction parameter, $$\frac{C_L \tan (C_L/C_{L,\alpha}) - \Delta C_D}{C_L \tan (C_L/C_{L,\alpha}) - C_L^2/(\pi AR)}$$
s	distance along section camber line
t	airfoil section local thickness
t_{max}	airfoil section maximum thickness
t_{max}^*	effective maximum thickness for attainable thrust calculations
Δu	longitudinal perturbation velocity difference across the wing lifting surface as a fraction of the free stream velocity
x, y, z	Cartesian coordinates
x'	distance in the x direction measured from the wing leading edge
x_1', x_2'	x' values at leading edge and trailing edge of wing element at element semispan
x_v'	x' value for center of detached leading-edge vortex flow
α	angle of attack of wing, in degrees

4

$\Delta\alpha_{ft}$ range of angle of attack for full theoretical thrust

α_{zt} angle of attack of wing giving a theoretical leading-edge thrust of zero for a specified wing spanwise station

β $\sqrt{1-M^2}$

γ ratio of specific heats

η location of maximum wing section thickness as fraction of chord

δ flap deflection angle in degrees

Λ sweep angle

Subscripts:

L   leading edge

n   measured normal to flap hinge line

o   original or first value

T   trailing edge

1,2   flap segment identifier

des   design condition

zt   zero thrust condition

hl   hinge line

C   cambered wing

F   flat wing

DEVELOPMENT OF COMPUTATIONAL SYSTEM

Expanded capabilities for the analysis and design of low speed flap systems are offered by recent modifications of an existing computer program introduced in reference 1. The revised program provides for the simultaneous analysis of up to 25 pairs of leading-edge and trailing-edge flap deflection schedules. Among other new features are a revised attainable thrust estimation method to provide more accurate predictions for low Mach numbers, and a choice of three options for estimation of leading-edge separation vortex flow effects.

The development of the basic computational system is covered in considerable detail in reference 1. That report describes numerical methods which have been incorporated into a computer program to permit the analysis of twisted and cambered wings of arbitrary planform with attainable thrust considerations taken into account. The computational system is based on a linearized theory lifting surface solution which provides a spanwise distribution of theoretical leading-edge thrust in addition to the surface distribution of perturbation velocities. In contrast to the commonly accepted practice of obtaining linearized theory results by simultaneous solution of a large set of equations, a solution by iteration is employed. The method also features a superposition of independent solutions for a cambered and twisted wing and a flat wing of the same planform to provide, at little additional expense, results for a large number of angles of attack or lift coefficients. A key feature of the superposition technique is the use of leading-edge thrust singularity parameters to identify and separate singular and nonsingular velocity distributions. This separation permits more accurate determination of leading-edge thrust and more accurate integration of pressure distributions for twisted and cambered wings of arbitrary planform. The following discussions will be concerned only with significant changes and improvements to the methods described in reference 1.

6

Leading-Edge and Trailing-Edge Flap Surfaces

The leading-edge and trailing-edge devices that may be treated by the present method are limited to "simple" hinged flaps. There is no provision for additional slats or for any separation between the flaps and the main wing surface.

In the revised program separate solutions for the longitudinal perturbation velocity distribution are made for both a leading-edge flap surface and a trailing-edge flap surface. These two additional surfaces cover the entire wing planform as do the two original surfaces for the flat and twisted and cambered wing. With this distinct separation of individual contributions to the overall wing loading distribution, it is a simple matter to combine loadings to cover not only a range of angles of attack but also a range of leading-edge and trailing-edge flap deflections.

For input flap surfaces, described as a spanwise distribution of flap chord and streamwise deflection angle, values of surface slope for each of the wing elements are determined within the program. Solutions for the longitudinal perturbation velocities corresponding to these new surfaces are performed simultaneously with the solutions for the flat and cambered wing. Because an assumption of lifting pressures proportional to the sine of the deflection angle rather than the tangent (the surface slope) is more reasonable, the lifting pressures are defined as:

$$C_p = 2\Delta u_F \ \frac{\sin \alpha}{\tan 1^\circ} \qquad \text{for the flat wing}$$

$$C_p = 2\Delta u_C \ \frac{\sin \delta_C}{\tan \delta_C} = 2\Delta u_C \cos \delta_C \qquad \text{for the cambered surface}$$

$$C_p = 2\Delta u_L \frac{\sin\delta_L}{\tan\delta_L} = 2\Delta u_L \cos\delta_L \qquad \text{for the leading-edge flap}$$

$$C_p = 2\Delta u_T \frac{\sin\delta_T}{\tan\delta_T} = 2\Delta u_T \cos\delta_T \qquad \text{for the trailing-edge flap}$$

For additional flap deflection angles, the user may specify factors m_L and m_T for the leading and trailing edges respectively:

$$\delta_L = \tan^{-1}(m_L \tan\delta_{L,o})$$
$$\delta_T = \tan^{-1}(m_T \tan\delta_{T,o})$$

where the subscript o indicates the original input flap deflections. In accordance with the assumption of lifting pressure proportional to the sine of the deflection angle, the flap induced lifting pressures are:

$$C_p = 2\Delta u_L \frac{\sin\delta_L}{\tan\delta_L}$$

$$= 2 m_L \Delta u_{L,o} \cos(\tan^{-1}(m_L \tan\delta_{L,o})) \qquad \text{for the leading-edge flap}$$

$$C_p = 2\Delta u_T \frac{\sin\delta_T}{\tan\delta_T}$$

$$= 2 m_T \Delta u_{T,o} \cos(\tan^{-1}(m_T \tan\delta_{T,o})) \qquad \text{for the trailing-edge flap}$$

Section force coefficients are found through the integration techniques described in reference 1. Now, however, the cambered wing coefficients include deflected flap as well as camber surface contributions. Both of these solutions are handled as described for the cambered surface in reference 1 except that, for the flap contribution, additional $\cos\delta_L$ and $\cos\delta_T$ terms are introduced. The following sketches illustrate the necessity for this correction. As shown in sketch (a) an incremental force for the cambered
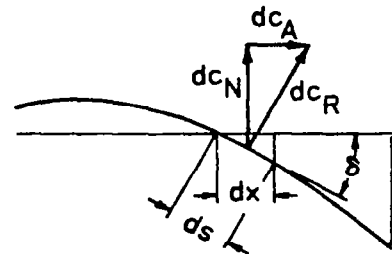
wing section may be defined as:

$$dc_N = dc_R \cos \delta$$

$$= \int C_p \, ds \cos \delta$$

$$= \int C_p \, dx$$

because $dx = ds \cos \delta$.
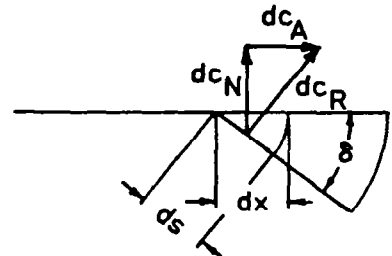
But for the flap surface shown in

sketch (b):

$$dc_N = dc_R \cos \delta$$

$$= \int C_p \, ds \cos \delta$$

$$= \int C_p \, dx \cos \delta$$

because $dx = ds$

Sketch (a)

Sketch (b)

These refinements, which introduce a cos δ term in both the lifting

pressure and the normal force coefficients for deflected flap surfaces, were

not used in the flap system study of reference 2. The cos δ correction and

the numerical method improvements afforded by the individualized treatment of

the deflected flap surfaces (instead of handling by methods designed specifi-

cally for generalized camber surfaces) are expected to increase the accuracy

of the program for application to flap systems.

Attainable Leading-Edge Thrust

The method for prediction of attainable leading-edge thrust described in

reference 3 was incorporated in the computer program of reference 1. That

method has been retained in the present revised program but has been modified

somewhat to be more applicable at the low Mach numbers sometimes encountered

in wind-tunnel testing. In general, the method described in reference 3 is

based on the use of simple sweep theory to permit a two-dimensional analysis, the use of theoretical airfoil programs to define thust dependence on local geometric characteristics, and the examination of experimental two-dimensional airfoil data to define limitations imposed by local Mach numbers and Reynolds numbers. The following discussion is concerned with a re-examination of experimental two-dimensional airfoil data and a redefinition of limitations imposed by local Mach numbers and Reynolds numbers. For a detailed discussion of the method the reader should consult reference 3.

In reference 3 limiting pressures, $C_{p,lim}$, were determined from corre-lations with two-dimensional airfoil experimental data covering Mach numbers from 0.3 to 0.9. To extend that range to lower Mach numbers, similar correlations for Mach numbers as low as 0.03 are shown in figure 1. Shown in figure 1(a) are axial force data from reference 4 covering a range of Reynolds numbers for airfoils of three thickness ratios at a Mach number of 0.061. The vertical dashed lines in figure 1(a) indicate that for angles greater than those indicated there was a large but undeterminable increase in axial force. Figure 1(b) gives data from reference 5 for two airfoils at various combinations of Mach numbers and Reynolds numbers. As in reference 3, values of $C_{p,lim}$ were found by iteration.

In figure 2(a), $C_{p,lim}$ values from figure 1 are plotted as a function of Reynolds number. The dashed line fairing of the data is intended to provide data for Reynolds numbers of 1 million and 3 million that can be plotted as a function of Mach number. Similar data from the original correlations of reference 3 are shown in figure 2(b). The arrows next to some of the data indicate that the $C_{p,lim}$ might be more negative than shown because the data did not show a definite break from the full thrust curve at

the highest angle of attack available in the data. In spite of considerable scatter in the data, general levels of the limiting pressure can be established and a trend of increasing limiting pressure with increasing Reynolds number for the lower Mach numbers is observable. More complete two-dimensional data would be desirable. There is a particular need for coverage of a greater range of angles of attack and Reynolds numbers.

Figure 3 shows $C_{p,lim}$ as a function of Mach number for three Reynolds numbers. The empirical data was obtained from the dashed line fairing of the data in the previous two figures. The empirical equation is intended to represent the general nature of the data. It has the same form as the equation given in the original development—differing only in the exponent, e. For normal Mach numbers greater than 0.3 the values are essentially the same as those given by the original equation.

The variation of $C_{p,lim}$, with Mach number and Reynolds number as given by the equation:

$$C_{p,lim} = \frac{-2}{\gamma M_n^2} \left[\frac{R_n \times 10^{-6}}{R_n \times 10^{-6} + 10^e} \right]^E$$

with $E = .05 + .35 (1-M_n)^2$

and $e = 4-3 M_n + 4 (1-M_n)^{15}$

is shown in figure 4. Note that $C_{p,lim}$ approaches the vacuum limit as the Reynolds number approaches infinity, and approaches zero as the Reynolds

number approaches zero. Because there is little data to provide guidance in selection of parameters for the equation below a normal Mach number of about 0.05, $C_{p,lim}$ is held constant at the $M_n = 0.05$ value from $M_n = 0.0$ to 0.05. In the new program, this equation replaces the original derived in reference 3.
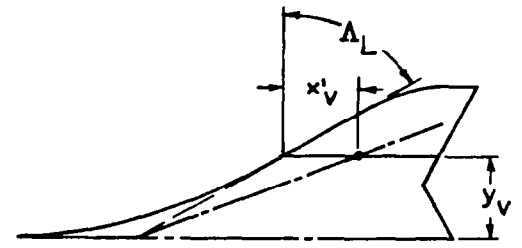
Vortex Force Distribution

The computer program of reference 1 accounts for a vortex force generated by detached leading-edge vortices which form when there is a failure to achieve full theoretical leading-edge thrust. In that program, the vortex force is assumed to act perpendicular to the wing reference plane at the wing leading edge and thus offers no contribution to wing axial force. That method is available to the program user as the default option, but there are two additional options in the present code. Both of these new options give an estimate of the distribution of the vortex force and provide contributions to the axial force as well as the normal force.

Option 1. For delta wings and delta wing derivatives, the vortex force center may be located through use of an empirical relationship derived with the aid of figure 5. In this figure, data from references 6 and 7 for uncambered delta wings with sharp leading edges are used to define, in an approximate fashion, the lateral location of the center of the vortex flow pressure field as a function of the wing local semispan (x cotΛ) and the angle of attack. The fairing of the data represented by the equation:

$$\frac{y_v}{x \cot\Lambda} = \frac{1}{1 + \sqrt{\tan \alpha}}$$

should be applicable to a range of sweep angles from about 50 degrees to about 80 degrees. As shown in sketch (c) it may be possible to provide an approximate

location of the center of the vortex pressure field even for wings with significant departures from the delta planform, and for wings which may employ twist and camber or deflected flaps. This may be accomplished by use of the equations:

Sketch (c)

$$x_v' = 0.0 \qquad\qquad (\alpha_{zt} - \Delta\alpha_{ft}) < \alpha < (\alpha_{zt} + \Delta\alpha_{ft})$$

$$x_v' = \frac{y}{\cot\Lambda_L} \sqrt{\tan(\alpha - \alpha_{zt} - \Delta\alpha_{ft})} \qquad\qquad \alpha > (\alpha_{zt} + \Delta\alpha_{ft})$$

$$x_v' = \frac{y}{\cot\Lambda_L} \sqrt{\tan(\alpha_{zt} - \Delta\alpha_{ft} - \alpha)} \qquad\qquad \alpha < (\alpha_{zt} - \Delta\alpha_{ft})$$

in which Λ_L is the local leading-edge sweep angle, α_{zt} is the wing angle of attack for local leading-edge thrust of zero, and $\Delta\alpha_{ft}$ is the range of angle of attack for full thrust. This formulation locates the vortex center aft of the leading edge only when full thrust is not realized. However, it does not account for the initiation of leading-edge separation at points along the leading edge other than the apex of the superimposed delta wing.

Option 2. An alternate and very simple means of locating the vortex force center is given by Lan in reference 8. When applied to the present numerical method the location of the vortex force center is:

$$x_v' = c_t \, c_{ave}$$

For both of the new options for vortex force location the distribution of the force is assumed to take the form shown in sketch (d). Mathematically this form can be expressed as:
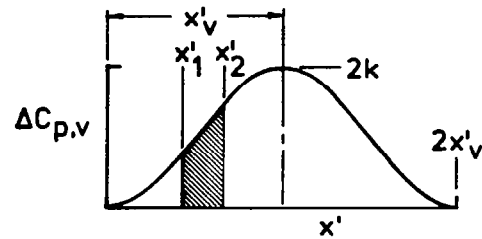
Sketch (d)

$$\Delta C_{p,v} = k\left(1 - \cos\pi \frac{x'}{x'_v}\right)$$

Over an element chord (x'_1 to x'_2) the incremental normal force due to the vortex is given by:

$$\Delta c_{N,v} = \frac{1}{c_{ave}} \int_{x'_1}^{x'_2} \Delta C_{p,v}\, dx$$

$$= \frac{k}{c_{ave}} \left[(x'_2 - x'_1) - \frac{x'_v}{\pi} \left(\sin \pi \frac{x'_2}{x'_v} - \sin \pi \frac{x'_1}{x'_v}\right) \right]$$

and over the entire interval from 0 to $2x'_v$:

$$\Delta c_{N,v} = \frac{1}{c_{ave}} 2kx'_v$$

so that:

$$k = \frac{\Delta c_{N,v}\, c_{ave}}{2x'_v}$$

The k factor establishes the magnitude of the $\Delta c_{p,v}$ distribution acting on the wing surface. Since the surface may be cambered and may include deflect-

14

ed flaps, there will be contributions to axial force as well as normal force. If the vortex center lies aft of the local chord midpoint, part of the vortex force will not affect the wing and will be lost.

Only limited advice regarding the selection of the vortex options can be offered at this time. The first option, with the vortex force acting perpendicular to the wing reference plane at the wing leading edge, was used in the correlations with experimental data given in reference 1. At large angles of attack, that approach seemed to overestimate the vortex effect—probably because much of the vortex field was actually aft of the wing surface rather than at the leading edge. The correlations with experimental data given in this report have been made using the second option. However, as discussed previously, this option is appropriate only for highly swept wings with delta or modified delta planforms. The authors have had no experience with use of the third option, the method given by Lan.

Angle of Attack Range for Full Thrust

As will be discussed in a later section of this report, it may be desirable for design purposes to know how much a local leading-edge flap deflection angle may be changed from the local flow alignment condition (presumed to be defined by α_{zt}) and still retain attached flow and full theoretical thrust. This angle of attack range may be found from the flat wing attainable leading-edge thrust calculations by setting the attainable thrust fraction K_t (defined by equation (9) in reference 3) equal to 1.0 and solving for $c_{t,n}$. Since $c_{t,n}$ is related to c_t (equation (5) in reference 3) and c_t is dependent on α (equation (15) in reference 1), the flat wing angle of attack at which thrust begins to be lost at any given span station may be calculated.

PROGRAM DESCRIPTION

The following description of the revised program will cover the entire listing of input data and program results even though much of this information is repeated from reference 1.

The computer program entitled "Aerodynamic Performance of Low Speed Wing Flap Systems" may be obtained for a fee from:

> Computer Software Management and
>   Information Center (COSMIC)
> 112 Barrow Hall
> University of Georgia
> Athens, GA 30602
> (404) 542-3265

Request the program by the designation LAR 13116. This program is written in FORTRAN IV for use on the Control Data 6600 and Cyber series of computers. Data are input in namelist form under the code INPT1.

The wing planform information is specified by a series of leading-edge and trailing-edge breakpoints. Up to 21 pairs of coordinates may be used to describe the leading edge and up to 21 pairs to describe the trailing edge. The planform input data in program terminology are:

NLEY   number of leading-edge breakpoints (limit of 21)

TBLEY   table of leading-edge y-values in increasing order of y from wing root to wing tip

TBLEX   table of leading-edge x-values corresponding to the TBLEY table

NTEY   number of trailing-edge breakpoints (limit of 21)

TBTEY   table of trailing-edge y-values in increasing order of y from wing root to wing tip

TBTEX   table of trailing-edge x-values corresponding to the TBTEY table

XMAX   largest x-ordinate occurring anywhere on the planform

SREF   wing reference area for use in aerodynamic force and moment coefficients

CBAR   wing reference chord for use in aerodynamic moment coefficients

16

XMC   x-location of moment reference center

ELAR   desired element aspect ratio (for flat and mildly cambered wings without flaps an element aspect ratio approximately one-half the full wing aspect ratio is recommended, for small chord flaps it may be necessary to use a larger element aspect ratio to place at least two elements within the chord)

The size of the wing in program dimensions is controlled by the entry:

JBYMAX   integer designating the number of elements in the spanwise direction (limit of 41)

The necessary scaling is done within the program by use of a scale factor

$2(JBYMAX)/(SPAN \times \beta)$. The number of complete wing elements N corresponding

to a given JBYMAX may be approximated as

$$N = 4 \times JBYMAX^2 \times \frac{ELAR}{\text{wing aspect ratio}}$$

The program has been written to accommodate 2000 right hand panel elements. Except in very special cases the JBYMAX integer will be much less than the limit of 41. The normal range is 10 to 20. Computational costs tend to increase as the square of the number of elements and the fourth power of JBYMAX.

The wing section mean camber surface must be specified by exactly 26 chordwise ordinates at up to 21 span stations. When fewer than 26 camber coordinates are used to define the sections, the ordinate tables must be filled with enough zeros to complete the list of 26. The necessary section information is:

NYC   number of spanwise stations at which chordwise sections are used to define the mean camber surface (limit of 21)

TBYC   table of y values for the chordwise camber surface sections, increasing order of y from root to tip

NPCTC   number of chordwise stations used in mean camber surface definition
             (limit of 26)

TBPCTC   table of chordwise stations, in percent of chord, at which mean
             camber surface ordinates are defined; in increasing order from
             leading to trailing edge

TZORDC   table of mean camber surface z-ordinates corresponding to the
             TBPCTC table; the full 26 values for the root chord (including
             zeros for values in excess of NPCTC) are given first, followed
             by similar information for all spanwise stations in increasing
             order of y

The TZORDC table may be multiplied by a scale factor TZSCALE if desired.

This may be useful if the original tabulated ordinates are nondimensionalized

with respect to a single measurement (the wing root chord, for example) or if

it is necessary to evauate the effect of change in camber surface severity.

The following wing section information is required for the calculation

of attainable leading-edge thrust.

NYR   number of spanwise stations at which airfoil section information
             is supplied (limit of 21)

TBYR   table of y values for airfoil section information, increasing
             order of y values from root to tip

TBTOC   table of airfoil maximum thickness as a fraction of the chord

TBETA   table of the section location of maximum thickness as a fraction of
             the chord

TBROC   table of the leading-edge radius as a fraction of the chord

The flight or test conditions are specified as:

XM   free-stream Mach number

RN   free-stream Reynolds number (based on $\bar{c}$) in millions, $R/10^6$

NALPHA   number of angles of attack to be calculated (limit of 12)

TALPHA   table of angles of attack to be calculated

NADRN   number of additional Reynolds numbers

TADRN table of additional Reynolds numbers (based on $\bar{c}$) in millions, $R/10^6$ (limit of 3)

IVOROP vortex location option

  0 full vortex force acts normal to wing reference plane of the wing leading edge, does not contribute to axial force

  1 vortex center given by empirical relationships derived from delta wing experimental data

  2 vortex center given by the method of Lan (ref. 8)

  (program defaults to 0)

   The following information will permit the calculation of loadings and forces on deflected leading-edge and trailing-edge flaps. If flap data is not desired, simply omit these entries.

NLEFY number of breakpoints in leading-edge flap chord distribution (limit of 20)

TBLEFY table of y values at breakpoints in leading-edge flap chord distribution, in increasing order of y from wing root to wing tip

TBLEFC table of leading-edge flap chords corresponding to the TBLEFY table

TBLEFD table of flap deflections in degrees (positive for leading edge down) corresponding to the TBLEFY table

NADLEFD number of leading-edge flap deflection multipliers, other than 1.0 (limit of 4)

TXMLEFD table of leading-edge flap deflection multipliers (applied as a multiplier of the tangents of the input flap deflections)

LEFTYPE type of leading-edge deflection

  1 for linear
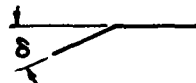
  2 for parabolic

  (program defaults to 1)

NTEFY   number of breakpoints in trailing-edge flap chord distribution
          (limit of 20)

TBTEFY   table of y values at breakpoints in trailing-edge flap chord
          distribution, in increasing order of y from wing root to wing tip

TBTEFC   table of trailing-edge flap chords corresponding to the TBTEFY
          table

TBTEFD   table of flap deflections in degrees (positive for trailing edge
          down) corresponding to the TBTEFY table

NADTEFD   number of trailing-edge flap deflection multipliers, other than 1.0
          (limit of 4)

TXMTEFD   table of trailing-edge flap deflection multipliers (applied as a
          multiplier to the tangents of the input flap deflections)

CLDES   lift coefficient for which flap system aerodynamic performance is
          to be optimized. Program aerodynamic characteristics are given
          only for angles of attack in the input TALPHA table unless CLDES
          is specified.

Spanwise tables must begin with y = 0 and extend to y = b/2 (with chords

of 0 where there are no flaps). At spanwise positions where there are dis-

continuities in either flap chord or deflection, it will be necessary to make

closely spaced tabular entries inboard and outboard of the discontinuity.

The program requires flap deflection angles measured in the x-z plane.

Flap deflection angles measured normal to the flap hinge line may be convert-

ed to program input angles by:

$$\delta = \tan^{-1} (\cos \Lambda_{hl} \tan \delta_n)$$

The program provides solutions for wing surfaces composed of all possi-

ble combinations of leading-edge and trailing-edge flap settings provided by

the original deflections (TBLEFD and TBTEFD) and by the flap deflection

multipliers (TXMLEFD and TXMTEFD). Up to 25 pairs of leading-edge and

trailing-edge flap deflection schedules may thus be treated simultaneously.

20

The program provides for a maximum of 50 iterations. If this number is reached without the convergence criteria being met, the results for the 50th iteration will be printed with a warning of the failure to meet criteria. If desired, the maximum number of iterations may be increased or decreased by the entry:

ITRMAX   maximum number of iterations

The program convergence criteria is met when, for all four wing surfaces and for two successive iterations, the average difference in perturbation velocity between iterations is less than one-half of one percent (0.005) of the average velocity over the wing. If the average velocity for the camber surface or either of the flap surfaces is less than the average velocity of the flat surface at 1° angle of attack, the flat wing surface value will be used instead. In many instances this criteria may be more stringent than necessary. If desired the convergence criteria may be changed by an entry:

CNVGTST   convergence criteria

The commonly accepted practice of performing subsonic calculations for a Mach number of 0.0 is not appropriate for this program. Realistic estimates of attainable thrust can be made only if both the Mach number and the Reynolds number correspond to actual conditions. In fact, the program will stop and write an error message to the user when XM = 0.0 is input.

The printed program results include:

(1) An iteration by iteration history of the convergence parameters.

(2) A listing of theoretical pressure distributions for the camber surface at 0° angle of attack and for the flat surface at 1° angle of attack. For each of the program spanwise stations (controlled by JBYMAX),

interpolated or extrapolated pressure coefficients are given for a set of chordwise stations.

(3) A listing of the spanwise distribution of section normal, axial, and pitching moment coefficients for the cambered wing at 0° angle of attack and the flat wing at 1° angle of attack. The interference axial force coefficient due to the flat surface loading acting on the camber surface and the theoretical thrust parameters $C_{t,F}$ and α_{zt} are also printed.

(4) A listing of wing overall theoretical aerodynamic coefficients C_N, C_A, C_M, C_L, and C_D with no thrust and with full theoretical thrust as a function of angle of attack.

(5) A listing of the spanwise distribution of the flat wing angle of attack range for full theoretical leading-edge thrust.

(6) A listing of wing overall estimated aerodynamic coefficients including C_N, C_A, and C_M for the basic pressure loading; ΔC_N and ΔC_A for attainable thrust and vortex force increments; and finally C_N, C_A, C_M, C_L, C_D, and S_S for the total loading.

Additional printed output data may be selected by use of the following print options:

IPRCPD = 1   theoretical pressure distributions for each of the selected angles of attack

IPRSLDT = 1   theoretical span load distributions of C_N, C_A, C_M, C_L, and C_D with no thrust and with full theoretical thrust for each of the selected angles of attack

IPRSLDA = 1   estimated span load distributions of C_N, C_A, C_M, C_L, and C_D with attainable thrust and vortex force effects for each of the selected angles of attack

IPRALL = 1   the preceding print control options apply to only the first
              set of flap deflections. Select this option if the three
              preceding options are to apply to all of the flap
              deflection combinations. Selection of this option could
              result in a very large volume of printed output.

PROGRAM APPLICATION

Among the program application topics to be covered in the following
discussions are correlation of program and experimental data, the influence
of Reynolds number on aerodynamic performance, and suggestions for use of the
program in an iterative fashion for flap system design.

Correlation of Program and Experimental Data

The correlations of program data and experimental data contained in this
report are intended to serve two purposes. The first is to demonstrate the
applicability of the programmed numerical methods to the aerodynamic analysis
of flap system test data obtained at a reasonably large Reynolds number. The
second is to show the dependence of wing aerodynamic performance on Reynolds
number conditions.

No estimate of skin friction and form drag contributions to the coeffi-
cients have been made. For the comparison with experimental data shown in
this report, the sum of these two contributions, $C_{D,0}$, has been set equal
to the experimental zero lift drag coefficient for the flat wing version of
the configuration. Separated vortex effects have been estimated by use of
the second option (IVOROP=1) described in the "Program Description" section.

Correlations of program results with unpublished experimental data for
an uncambered arrow wing supersonic cruise configuration with leading-edge
and trailing-edge flaps are shown in figure 6. These are the same data that
were used in reference 2. A number of refinements in the present program

which were not considered in the calculations of that reference provide a better correlation with the experimental data. In particular, the axial force correlations are noticeably improved. The normal force prediction is also changed, but in such a way that there is only a slight improvement in the drag prediction for the lift coefficient range of interest.

The data for the wing with no flap deflections show a slight underestimation of the leading-edge thrust achieved and some underestimation of the normal force. Generally, however, the method provides a reasonably good prediction of the drag relative to the full and no thrust values.

Figures 6(b) through 6(d) show data for a series of leading-edge flap deflections with the trailing-edge flaps at 10°. Notice, in particular, the behavior of the axial force data. The large negative values of the axial force achieved in the experiment and generally well predicted by the program are responsible for the improved wing performance with increasing flap deflection. Note the decreasing potential for leading-edge thrust (the difference between the no thrust and full thrust curves) as the leading-edge flap deflection is increased. The attainable thrust prediction method is seen to give a good estimate of the degree of thrust actually achieved. The program data indicate that increasing the flap deflection beyond 40° would produce some small additional performance gains. The experimental data, however, show little or no gain in performance for the 40° flaps compared to the 30° flaps. It is probable that linearized theory methods will generally overestimate the benefits of large flap deflections.

Figures 6(c), 6(e), 6(f), and 6(g) form a series in which the trailing-edge flap deflection varies while the leading-edge flap remains set at 30°. Notice that in this set of data the axial force shows a considerable change

in the general level but only a small change in shape. Generally, there is good agreement between the program prediction and the experimental data up to 30° flap deflection. At 40° the correlation is poor. The reason for this failure is evident in the normal force correlation; the trailing edge flap has lost effectiveness. The normal force generated at 40° is not appreciably greater than that generated at 30°.

Experimental data from reference 9 shown in figures 7 and 8 point out the dependence on Reynolds number of wing aerodynamic performance. Data for a wing-body combination with an aspect ratio 4 flat delta wing with an NACA 0005-63 section are shown in figure 7. The experimental data are compared with linearized theory program results for no leading-edge thrust and full leading-edge thrust as well as with present method data which include attainable thrust and vortex force estimates. The data for both Reynolds numbers show a reasonably good correlation of the program data, labeled present method, with experimental data at least up to about 10 degrees angle of attack or a lift coefficient of about 0.6. The effect of Reynolds number on axial force and drag appears to be predicted adequately by the present method. Correlations for the same configuration with a twisted and cambered wing instead of a flat wing are shown in figure 8. For this wing, predictions given by the present method are good only up to about 7.5 degrees or a lift coefficient of about 0.5 at the lower Reynolds number, but are good up to about 10 degrees or a lift coefficient of 0.65 at the higher Reynolds number. The difference is most apparent in the axial force curve. At the higher Reynolds number the critically important axial force behavior is given quite well over an angle of attack range from about -8.0 to +10.0 degrees.

An example of the effect of Reynolds number on the pitching moment of
these two wing-body models is given in figure 9. The flat wing pitching
moment curve shows a break from the predicted curve at about 6 degrees for
the lower Reynolds number. At the higher Reynolds number this break is
delayed to about 8°. In contrast to this mild improvement, the cambered wing
data show a dramatic improvement with the increase in Reynolds number. The
break in the pitching moment curve has been delayed from about 6 degrees to
12 degrees or higher. These data show that twisted and cambered wings are
far more sensitive to Reynolds number effects than are flat wings. The good
agreement between program results and experimental pitching moment data at
the higher Reynolds number appears to be very promising. However, as of yet,
few other pitching moment correlations have been made to test the general
applicability of the method.

Reynolds Number Limitations

The experimental force data examined in the preceding section of this
report showed a greater effect of Reynolds number on twisted and cambered
wing performance than on flat wing performance. An examination of pressure
distributions and limitations on peak suction pressures shows that wings with
leading-edge flaps as well as twisted and cambered wings can generally be
expected to have a greater sensitivity to Reynolds number than flat or
uncambered wings of the same planform.

Figures 10 to 12 give examples of the effect of Reynolds number on
achievable peak pressures. In all of these figures, C_p is shown as a
function of the square root of the x ordinate to chord ratio in order to
accentuate the leading-edge region. These distributions are shown for a
series of angles of attack so that the approach to a limiting pressure and

the subsequent collapse of the pressure peak may be observed. In addition, limiting pressures as defined by the empirical attainable leading-edge thrust technique are indicated. In figure 10, data for a two-dimensional airfoil from reference 10 are shown for Reynolds numbers from 0.1×10^6 to 3.1×10^6. These data show a strong dependence on Reynolds number of the magnitude of the peak pressures achievable. The negative pressure peak for the largest Reynolds number appears to be about two and one-half times greater than that for the lowest Reynolds number. Limiting pressures given by the attainable thrust prediction method of reference 3 are also shown on this figure. These limiting pressures serve merely as a device for accounting for thrust losses observed in experimental force data for two-dimensional airfoils. The attainable thrust limiting pressures actually account for two factors which limit thrust: the failure to attain theoretical peak suction pressures and also the tendency of these peaks to occur at a more rearward position on the airfoil. Thus, it is not surprising that the attainable thrust limiting pressures are less than the actual peak pressures. Even with this discrepancy, however, the attainable thrust limiting pressures should be valuable in prediction of trends due to changes in Mach number and Reynolds number. The data for a swept semispan wing (ref. 11) in figure 11 and the data for wing-body configuration (ref. 12) in figure 12 show similar trends and about the same relationship of actual pressure peaks to the attainable thrust limiting pressures.

The performance of wings with sharp leading edges is generally believed to be insensitive to changes in Reynolds number. This appears to be true for flat highly swept delta wings, but the generalization may not hold for wings with sharp leading-edge flaps deflected so as to minimize separation.

Research data collected for use in the analysis of wind energy systems (reference 13) can be of use in a study of the problem. In that research, it is necessary to consider the behavior of airfoils in reversed as well as forward motion. Typical lift curve data for a range of Reynolds numbers are shown in figure 13. The airfoil in reversed flow, of course, has a very sharp leading edge. These data indicate that only above angles of attack of 8 to 10 degrees is the sharp leading-edge airfoil C_L appreciably less sensitive to Reynolds number changes than the rounded leading-edge airfoil C_L. For smaller angles of attack, C_L changes are actually larger for the sharp leading-edge section than for the rounded leading-edge section. Thus, within this Reynolds number range, there will be important Reynolds number sensitivities for sharp leading-edge flaps if the local angle of attack must be restricted to small values to prevent separation. For the rounded leading-edge airfoil there are likely to be further increases in C_L with increases in Reynolds number above 1.8 million (the lift curve slope for R=1.8 million is still below the potential theory value). For the sharp leading-edge airfoil, increases in C_L with increases in Reynolds number above 1.8 million are likely to occur only for angles above about 6° (up to this point the lift curve for R=1.8 million matches the potential plus vortex lift theory). There is a need for data covering a larger range of Reynolds numbers and for data applicable to airfoil sections with sharp trailing edges as well as sharp leading edges. Highly swept flat wings with sharp leading edges apparently are relatively insensitive to Reynolds number changes, even at low Reynolds numbers, because the large growth of upwash along the leading edge causes the outboard wing sections to operate at large effective angles of attack where Reynolds number effects are insignificant.

The special importance of Reynolds number effects on the performance of twisted and cambered wings and wings with leading-edge flaps may be illustrated with the aid of two sketches. In sketch (e) is shown a section of a flat wing with superimposed pressure distributions for two Reynolds numbers. The shaded portion of the pressure loading and the shaded force arrow represent the effect of an increase in Reynolds number. The force arrows at the right represent the resultant pressure force on the section at the lower Reynolds number and the increase in this force due to the increase in Reynolds number. These two forces act in generally the same direction, normal to the wing surface, and thus there is only a small improvement in the lift-drag ratio due to the increase in Reynolds number.
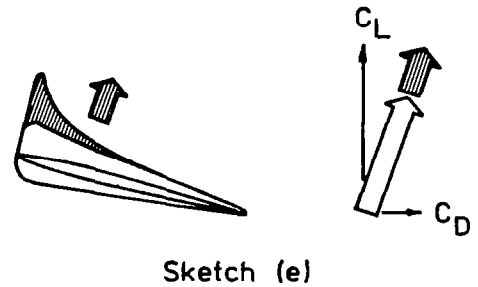
Sketch (e)

For a wing with a leading-edge flap (or a wing with leading-edge camber) the situation can be quite different as illustrated in sketch (f). For such a wing section to perform efficiently the flap must carry a significant load so as to produce a force with a thrust component. This loading will be similar to the loading on the forward portion of a flat wing. As shown by the shaded portion of the pressure distribution and the shaded force arrow, here too, Reynolds

Sketch (f)
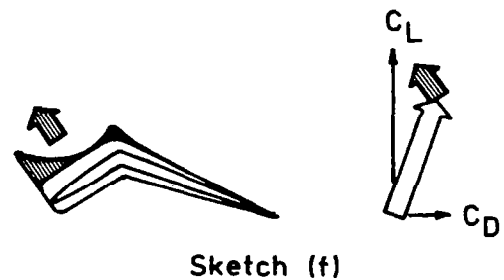
number could have a substantial influence on the force generated. But as shown in the resultant pressure force vectors at the right, the additional force due to the increase in flap loading with Reynolds number, which acts normal to the flap surface, can have a relatively large effect on the resultant drag and the lift drag ratio.

From this discussion, it can be seen that there is a special need for high Reynolds number testing of candidate flap systems. Inadequate Reynolds number test conditions could lead not only to poor prediction of flight performance but also could result in rejection of flap systems with excellent high Reynolds number performance but poor low Reynolds number performance. Unfortunately, results from the present study do not provide firm guidelines for acceptable test Reynolds numbers.

An effort to introduce pressure limiting based on the attainable thrust method into the present computer program was not successful. A severe deterrent to such measures is the sometimes drastic collapse of the pressure peak as illustrated in figure 14. The data from reference 5 show an extreme change in the shape and magnitude of the pressure distribution between the angles of attack of 9 and 10 degrees.

Effective Thickness and Leading-Edge Radius

For any of the wide variety of NACA "standard" airfoils the attainable thrust calculations are naturally based on the listed values of airfoil thickness and leading-edge radius. The attainable thrust method was calibrated with airfoils such as these. However, for nonstandard airfoils (for example, blunted circular arc sections) direct use of the geometric thickness and radius may lead to erroneous results. A method for obtaining the effective thickness and radius for these problem airfoils is outlined in the following discussion.

Airfoils on which the method is based have a family resemblance. The leading-edge radius and thickness interdependence may be approximated as:

$$\frac{r}{c} \approx \frac{0.28}{\eta} \left[\frac{t_{max}}{c}\right]^2$$

and the thickness distribution follows the general form shown in sketch (g) which with little error may be represented as:

$$\frac{t}{t_{max}} = 1.0 - \left[1.0 - \sqrt{\frac{x'/c}{\eta}}\right]^{1.5}$$
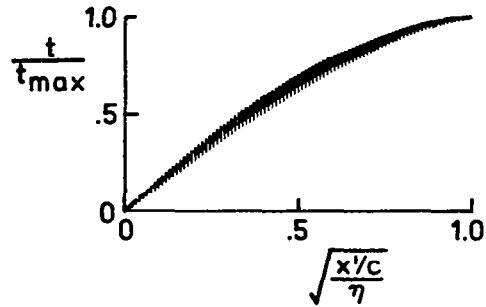
Sketch (g)

The leading-edge radius is actually a measure of the rate of growth of thickness over much of the forward portion of the airfoil rather than a localized leading-edge characteristic only.

The preceding family relationships may be used to obtain effective thickness and radius values for arbitrary sections through the following steps illustrated in sketch (h).
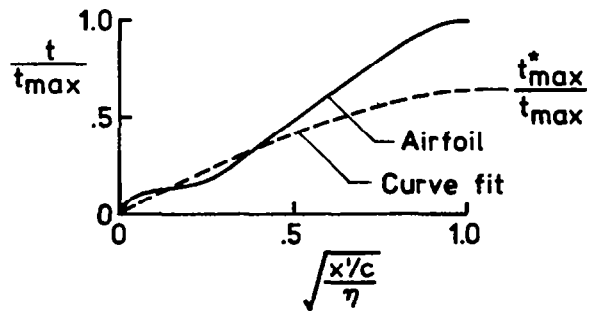
(1) Plot airfoil ordinates in the form

$$t/t_{max} \quad vs \quad \sqrt{\frac{x'/c}{\eta}}$$

Sketch (h)

(2) Fit a curve of the form

$$\frac{t}{t_{max}} = \frac{t_{max}^*}{t_{max}} \left\{ 1.0 - \left[1.0 - \sqrt{\frac{x'/c}{\eta}}\right]^{1.5} \right\}$$

31

by selecting a value of t^*_{max} to match as closely as possible the actual airfoil ordinates with particular emphasis on the forward half of the plot.

(3) Use the effective thickness t^*_{max} to obtain an effective thickness ratio

$$\frac{t^*_{max}}{c} = \frac{t^*_{max}}{t_{max}} \frac{t_{max}}{c}$$

and an effective leading-edge radius to chord ratio

$$\frac{r^*}{c} = \frac{.28}{\eta} \left[\frac{t^*_{max}}{c}\right]^2$$

Substitution of these effective values of thickness and radius for the pure geometrical quantities should result in more accurate estimation of attainable thrust.

Special Handling of Small Span Flaps

In the numerical solution for pressure loadings on deflected flap surfaces there may be a poor representation of the flap if the flap span covers only a few program element spans. Program surface slopes are assumed to be constant over any given program element with the value being determined at the element mid semispan. For some cases, the program user may want to adjust input flap geometric inputs so that the program flap area will provide a better representation of the actual flap area. As shown in sketch (i) this may be accomplished by altering the location of flap chords to correspond to the program spanwise grid spacing b/2(JBYMAX) and changing the flap chords to preserve the area.

Actual

Adjusted

Sketch (i)

32
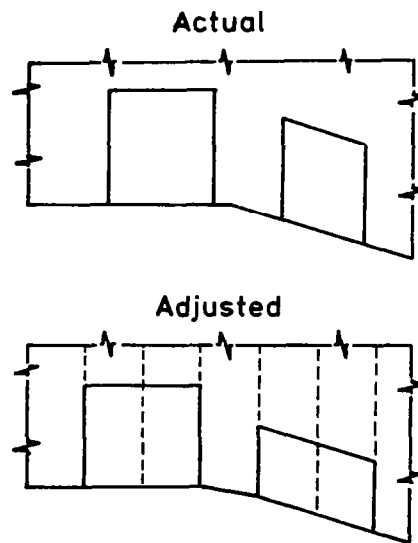
Flap System Design Notes

The flap system design notes discussed herein are based on the concept that the primary purpose of the flaps is the generation of a specified lift with an aerodynamic efficiency comparable to that which could be attained by the flat wing with full theoretical leading-edge thrust. Properly designed leading-edge flaps can provide a substitute for the leading-edge thrust which often cannot actually be realized. This is accomplished by a loading of the deflected surface which produces a distributed rather than a concentrated thrust force. Trailing-edge flaps serve to reduce the angle of attack required to produce the specified lift and since they affect the span load distribution they may also influence the lifting efficiency.

A supersonic cruise configuration illustrated in sketch (j) will be taken as an example to illustrate the application of design techniques made possible by features of the present computer program. This is a wing-fuselage configuration with a twisted and cambered wing designed for C_L=0.10 at M=2.7. Landing approach design conditions have been chosen at:

Sketch (j)

$$M = 0.25$$

$$R = 160 \times 10^6$$

$$C_L = 0.55$$

$$\alpha = 8°$$

The trailing-edge flaps on either side of the airplane (between the fuselage and the inboard engine, and between the inboard and the outboard engine) are fixed in planform but may be deflected as necessary. It is assumed for this example that trailing-edge devices for the remainder of the wing will be employed as ailerons for roll control and will be unavailable for use in generating lift. This configuration was previously used in the study reported in reference 2. As will be seen in the following discussions, corrections and refinements to the computational techniques alter to some degree the results of the previous study.

Because the purpose of the leading-edge flaps is the restoration of performance benefits lost due to the failure to achieve leading-edge thrust, it is first necessary to estimate the extent of full thrust achievement for the basic wing. This may be done in the following manner.

For the basic wing (which includes a distribution of twist and camber for a supersonic cruise design condition), the program provides an estimate of the spanwise distribution of the wing angle of attack for zero local leading-edge thrust as shown in sketch (k). At a given span station, this angle of attack is estimated to produce a stagnation point at or near the local airfoil origin. Local thrust will be generated only at angles of attack larger or smaller than the angle of attack for zero thrust. For a flat wing, α_{zt} will be zero at all span stations. A well designed twisted and cambered wing will have a nearly constant α_{zt} across the span at the design Mach number.
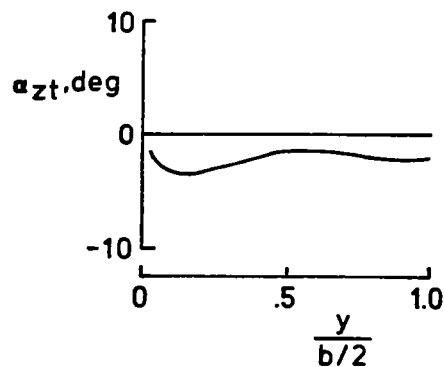
Sketch (k)

For a flat wing of the same planform, the program provides an estimate of the spanwise distribution of the range of angle of attack for full thrust as shown in sketch (l). For angles outside this range, the attainable thrust prediction method indicates attainable thrust less than the full theoretical values.
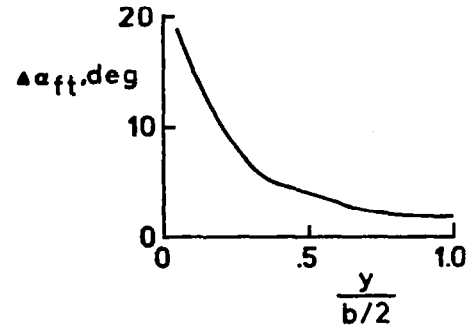
A combination of basic wing α_{zt} and flat wing $\Delta\alpha_{ft}$ gives a plot of the range of full thrust for the basic wing as shown in sketch (m). The shaded region indicates the total range of angles of attack that are estimated to result in full theoretical thrust. Generally, as shown here, the range of full thrust will not cover the design angle of attack. For portions of the wing semispan where the range of full thrust falls below the design angle of
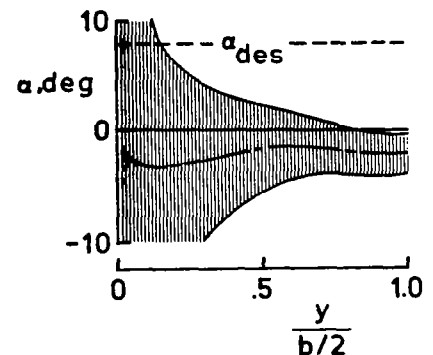
Sketch (l)

Sketch (m)

attack, leading-edge flaps will be required. As a rough guide, the product of the flap chord and the flap deflection angle should be proportional to the discrepancy between the upper limit of the full thrust range and the design angle of attack. This sketch indicates that leading-edge flaps are required for span stations beyond about the 0.15 semispan position. In contrast, the study of reference 2 indicated that the flaps were needed only beyond the 0.30 semispan position. The difference is due to the newer and more accurate

method of estimating attainable thrust for low values of the Mach number normal to the leading edge. For the inboard wing panel of this example, the normal Mach number is 0.071.

The foregoing considerations led to selection of a candidate leading edge flap system shown in sketch (n). For the wing outer panel, flap chords were constrained by structural considerations. Nominal streamwise deflection angles of 20° were chosen for both leading-edge and trailing-edge flaps. The computer program was used to estimate the aerodynamic efficiency of the flap system as represented by the suction parameter, S_s. The results shown in figure 15 cover a range of leading-edge and trailing-edge flap settings from 0 to 40 degrees. The solid contour lines depict constant values of the suction parameter, and the dashed contour lines show the required angle of attack for the design lift coefficient. Subject to the design angle of attack of 8° restraint, the performance is estimated to optimize at a trailing-edge flap angle of about 22° and a leading-edge flap angle of about 24°. Linearized theory probably tends to overestimate the benefits of leading-edge flap deflection, so that the actual optimum deflection may be somewhat less than 24°—perhaps about 20°.
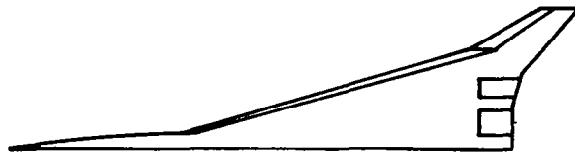
As the design by iteration process is conducted, an occasional check of the span load distribution is warranted. A program estimate of the span load

Sketch (n)

36

distribution for the candidate flap system with 20° deflections of both leading-edge and trailing-edge flaps is shown in sketch (o). This curve is compared with the well known idealized elliptic span load distribution (the dashed line). The shape of the span load distribution is controlled to a large degree by the wing planform, but trailing-edge flap deflections can provide some degree of modification. The idealized distribution could be approached more closely if trailing-edge flaps could be employed for the outer portion of the wing semispan, but this is not allowed by the design guidelines. The study of reference 2 showed a significant improvement in performance when this requirement was ignored to allow trailing-edge flaps to cover the entire span.
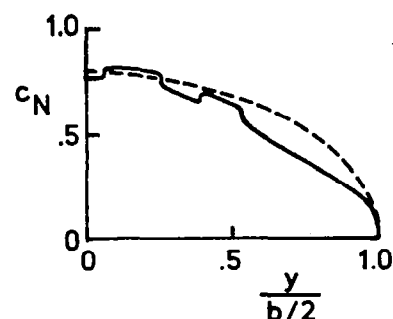
The candidate leading-edge flap design based on attainable thrust considerations employs a constant deflection angle for the entire length of the flap. Figure 16 was prepared as a means of judging possible improvements with other deflection schedules. Section drag-due-to-lift factors have been plotted as a function of the leading-edge flap deflection. To eliminate the intermingling of curves that otherwise would occur, the drag due-to-lift factors shown are increments relative to the zero leading-edge deflection values. For the outer flap panel (outboard of the 0.726 station) the optimum deflection angles are generally less than for the inner panel. To explore the possibility of improved performance, the program was rerun with nominal deflection angles of 22.7° and 17.2° for the inboard and outboard panels respectively instead of the constant 20° angle. The results showed a very

Sketch (o)

slight decrease in performance rather than an increase. This perhaps indicates only the very complex nature of the interactions involved in camber surface design. Increased inboard flap deflections reduce the inboard lift and thus reduce the upwash field which the outboard flap utilizes for performance gains. A reversal of the deflection schedule to 17.2° inboard and 22.7° outboard resulted in a slight gain in performance. But because this schedule would result in a gap between the edges of the inboard and outboard flap, the original constant 20° deflection was retained. It appears that section drag-due-to-lift factor patterns, such as those shown in figure 16, which enhance outboard flap performance, are a desired feature of good flap design.

The previously discussed plots of the range of full thrust may be used to give some indication of the flap system flow separation characteristics as shown in figure 17. These plots are given for leading-edge flap deflections of 0°, 20°, and 40°, and for a trailing-edge flap deflection of 20°. The program estimates cover flight conditions and representative wind-tunnel conditions. Angles of attack required to generate the design lift coefficient of 0.55 are shown by the dashed lines. For undeflected leading-edge flaps, the program data indicate that full thrust would be achieved only over the inboard 20 percent of the semispan at flight conditions. Thus, leading-edge flow separation and the formation of a detached leading-edge vortex system could be expected over the major portion of the wing. However, even with a large amount of detached flow the program can be expected to give good estimates of wing performance for flat wings, because the loss of leading-edge pressure peaks and the associated vortex formation have little effect on the direction of the resultant force. With leading-edge flap deflection increased

to 20°, the separation point is estimated to move to about the midpoint of the wing semispan for flight conditions. At a 40° deflection, attached flow over the entire wing is indicated. However, the 40° deflection is well beyond the estimated optimum of about 24° given by the program (see figure 15). A leading-edge flap deflection greater than that necessary to just bring the upper limit of the full thrust range to the design angle of attack is counter productive. At larger angles, the thrust will decrease and the axial force component of that thrust will also decrease. Furthermore, it is likely that the benefits of increased flap deflection will in actuality fall off more rapidly than program results predict. Thus, more attention should be given to deflection angles somewhat less than the program optimum. A 20° deflection angle might be a good compromise. Although some degree of flow separation is indicated for the 20° deflection, the effect on performance could be fairly small if the vortex induced pressures were to act for the most part on the deflected surface. This could happen in cases where there is a difference of only a few degrees between the upper limits of the full thrust region and the angle of attack for the design C_L. The program gives an estimate of the distribution of the vortex pressure field (options 1 and 2); but, unfortunately, this is one of the least reliable of the program features. Experimental evaluation also poses a dilemma. As indicated here and as discussed previously, flow separation is very sensitive to the Reynolds number. High test Reynolds numbers are required, but there is no sure way of establishing an acceptable level.

The degree of leading-edge thrust achieved can be controlled by selection of airfoil parameters. Within limits imposed by other design requirements, the thrust can be increased by increasing the section thickness

and leading-edge radius. Conversely, the thrust can be minimized and the leading-edge separation vortex force maximized by introducing a sharp leading edge. A question that often arises in flap system design is: Under what circumstances should the leading edge be deliberately sharpened so as to create leading-edge separation vortex flow? The following discussion may provide a better understanding of the problem.

Sketch (p) shows a deflected leading-edge flap and the axial force vectors that result from the attainable thrust and from the vortex force, provided that the vortex field remains totally on the deflected surface. The change in the section axial force coefficient due to a change in the attainable thrust may be expressed as:

$$dc_A = -dc_{t,a} \cos \delta_L + dc_{t,a} \frac{\sin \delta_L}{\cos \Lambda_L}$$

or
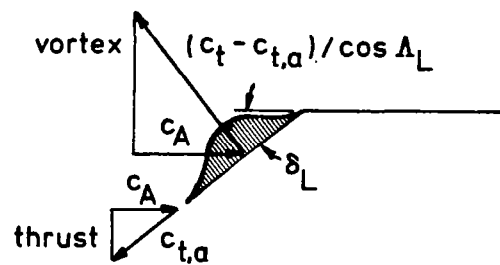
$$\frac{dc_A}{dc_{t,a}} = \frac{\sin \delta_L}{\cos \Lambda_L} - \cos \delta_L$$

Thus, there is no change in the axial force with a change in the attainable thrust when:

$$\delta_L = \tan^{-1} (\cos \Lambda_L)$$

If the deflection angle is measured normal to a hinge line which is parallel to the leading edge there is no change in the axial force with a change in the attainable thrust when:

$$\delta_{L,n} = \tan^{-1} (\tan \delta_L / \cos \Lambda_L) = 45°$$

For smaller deflection angles, axial force will be reduced by an increase in the attainable thrust. For larger deflection angles, axial force will be reduced by an increase in the vortex force. Sketch (q) shows the critical streamwise deflection angle and the regions in which either an increase in the thrust or an increase in the vortex force will result in reduced axial force and improved aerodynamic performance. For wing sweep angles up to 50° or 60°, the critical streamwise flap deflection angle is quite large, and it is unlikely that sharp leading-edge flaps would offer any benefits. But, for
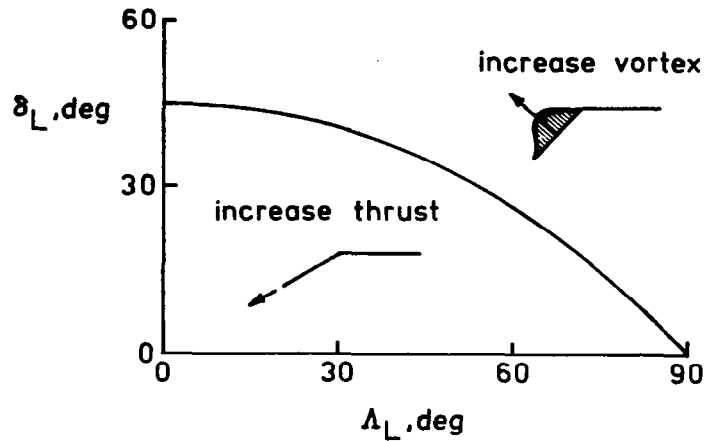
Sketch (q)

wing sweep angles of 60° to 70° and more, sharp edges may indeed offer performance benefits. As mentioned previously, this simple analysis is appropriate only if the separated vortex flow is confined to the deflected flap surface. A larger extent of separated flow would increase the critical angle and make leading-edge sharpness less attractive. Because the vortex center tends to move rapidly from the leading-edge as the angle of attack is increased (see figure 5), the incremental angle of attack ($\alpha_{des} - \alpha_{zt}$) producing detached flow must be limited to small values. On the other

hand, this simple analysis ignores the changes in the section normal force. Consideration of this factor would tend to reduce the critical angle and make sharp leading edges relatively more attractive. Thus the critical angle variation shown as a line on sketch (q) should probably be a band separating the areas where an increase in thrust or an increase in vortex force will result in improved performance. In any case, this plot serves only as an indicator of the advisability of considering leading-edge changes.

The inboard wing panel of the configuration used in the illustrative design problem has a leading-edge sweep angle of 73° and a critical flap deflection angle of 16.3°. Thus, it might appear that the wing performance could be improved by resorting to a sharp leading edge. However, according to the same criteria, the outer wing panel with its 60° sweep angle requires a rounded leading edge. Since the larger portion of the leading-edge flap performance gains are generated by the outer panel flap operating in a strong upwash field, it would seem that outer panel requirements should take precedence. Sharp edge induced flow separation on the inboard panel leading edges would tend to reduce the upwash at the outer panel leading edges.

The computer program appears to be applicable to the analysis and design of wings with appreciable leading-edge radius over a large range of angles of attack and a large range of flap deflection angles, provided that the Reynolds number is large enough to insure attached flow over the major portion of the wing. For wings with sharp leading edges, the range of applicability may be more restricted. The program can be expected to give reasonably good predictions of aerodynamic characteristics for flat wings and wings with mild camber surfaces. But for sharp leading-edge wings with deflected flaps, good predictions can be expected only if the separated leading-edge flow reattaches

ahead of the leading-edge flap hinge line. Sketch (r) will help to explain

the reason for this limitation.

The sketch shows a typical section lifting

pressure distribution given by the program

for a twisted and cambered wing with de-

flected leading-edge and trailing-edge

flaps. Note the strong singularities at

the hinge lines of the leading-edge flap

and the trailing-edge flap. If the real

flow separates and does not reattach for-

ward of the hinge line, these loading
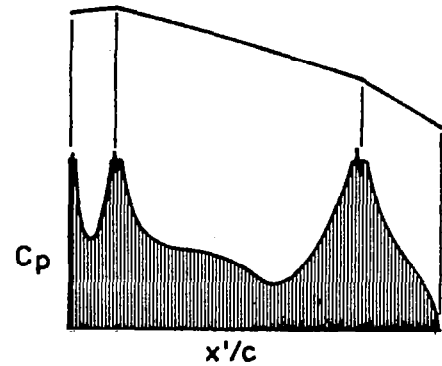
peaks will not be realized. Thus with a

strongly detached flow, both leading-edge and trailing-edge flaps will lose

effectiveness. As discussed previously, an attempt to introduce pressure

limiting into the program was not successful. Thus, the program will tend to

predict better aerodynamic performance than can actually be achieved under

conditions which promote strong flow detachment. Fortunately, it also

appears that the better the wing aerodynamic performance, the more likely it

is that the program will be capable of predicting that performance.

C_p

x'/c

Sketch (r)

CONCLUDING REMARKS

This report describes the recently expanded capabilities for analysis

and design of low speed flap systems afforded by a computer program introduc-

ed in reference 1. The present method provides for the simultaneous analysis

of up to 25 pairs of leading-edge and trailing-edge flap deflection

schedules. Among other new features of the program are a revised attainable

43

thrust estimation method to provide more accurate predictions for low Mach numbers, and a choice of three options for estimation of separated leading-edge vortex flow effects.

Comparison of program results with low speed experimental data for an arrow wing supersonic cruise configuration with leading-edge and trailing-edge flaps shows good agreement over most of the range of flap deflections. Correlations of program and experimental data for a delta wing-body model employing twist and camber showed a significant effect on wing performance of an increase in test Reynolds number from 1.5×10^6 to 8.0×10^6. At the higher Reynolds number the program provided good estimates of the aerodynamic lift, drag, and pitching moment characteristics. These force data comparisons as well as an independent study of the effects of Reynolds number on airfoil and wing pressure distributions show that the aerodynamic performance of twisted and cambered wings and wings with leading-edge flaps can be expected to be much more sensitive to Reynolds number effects than the aerodynamic performance of flat wings. Thus there is a special need for high Reynolds number testing of candidate flap systems. Inadequate Reynolds number test conditions could lead not only to poor prediction of flight performance but also could result in rejection of flap systems with excellent high Reynolds number performance but poor low Reynolds number performance.

Suggestions for use of the program in an iterative manner for the design of efficient leading-edge and trailing-edge flap systems have also been advanced. The design goal is the definition of flap systems which are no larger and no more complex than necessary to produce an aerodynamic efficiency comparable to that which could be attained with flat wing full theoretical leading-edge thrust if there were no Reynolds number limitations.

44

REFERENCES

1. Carlson, Harry W.; and Walkley, Kenneth B.: A Computer Program for Wing Subsonic Aerodynamic Performance Estimates Including Attainable Thrust and Vortex Lift Effects. NASA CR-3515, 1982.

2. Carlson, Harry W.: Application of an Aerodynamic Analysis Method Including Attainable Thrust Estimates to Low Speed Leading-Edge Flap Design for Supersonic Cruise Vehicles. NASA CR-165843, 1982.

3. Carlson, Harry W.; Mack, Robert J.; and Barger, Raymond L.: Estimation of Attainable Leading-Edge Thrust for Wings at Subsonic and Supersonic Speeds. NASA TP-1500, 1979.

4. Jacobs, Eastman N.; and Sherman, Albert: Airfoil Section Characteristics as Affected by Variations of the Reynolds Number. NACA Report 586, 1937.

5. McCullough, George B.: The Effect of Reynolds Number on the Stalling Characteristics and Pressure Distributions of Four Moderately Thin Airfoil Sections. NASA TN-3524, 1955.

6. Marsden, D. J.; Simpson, R. W.; and Rainbird, W. J.: An Investigation Into the Flow Over Delta Wings at Low Speeds With Leading Edge Separation. Rep. No. 114, The College of Aeronautics, Cranfield (England), February 1958.

7. Wentz, W. H., Jr.: Effects of Leading-Edge Camber on Low-Speed Characteristics of Slender Delta Wings. NASA CR-2002, 1972.

8. Lan, C. Edward; and Chang, Jen-Fu: Calculation of Vortex Lift Effect for Cambered Wings by the Suction Analogy. NASA CR-3449, 1981.

9. Hall, Charles F.: Lift, Drag, and Pitching Moment of Low-Aspect-Ratio Wings at Subsonic and Supersonic Speeds. NACA RM A53A30, 1953.

10. Pinkerton, Robert M.: The Variation with Reynolds Number of Pressure Distribution over an Airfoil Section. NACA Report No. 613, 1938.

11. Tinling, Bruce E.; and Lopez, Armando E.: The Effects of Reynolds Number at Mach Numbers up to 0.94 on the Loading on a 35° Swept-Back Wing Having NACA 65 A012 Streamwise Sections. NACA RM A52B20, 1952.

12. Fischetti, Thomas L.: Investigation at Mach Numbers From 0.80 to 1.43 of Pressure and Load Distributions Over a Thin 45° Sweptback Highly Tapered Wing in Combination With Basic and Indented Bodies. NACA RM L57D29a, 1957.

13. Jesch, L.F.; and Walton, D.: Reynolds Number Effects on the Aerodynamic Performance of a Vertical Axis Wind Turbine. Third International Symposium on Wind Energy Systems, Lyngby, Copenhagen, Denmark, August 26-29, 1980.

(a) $M_n = .061$
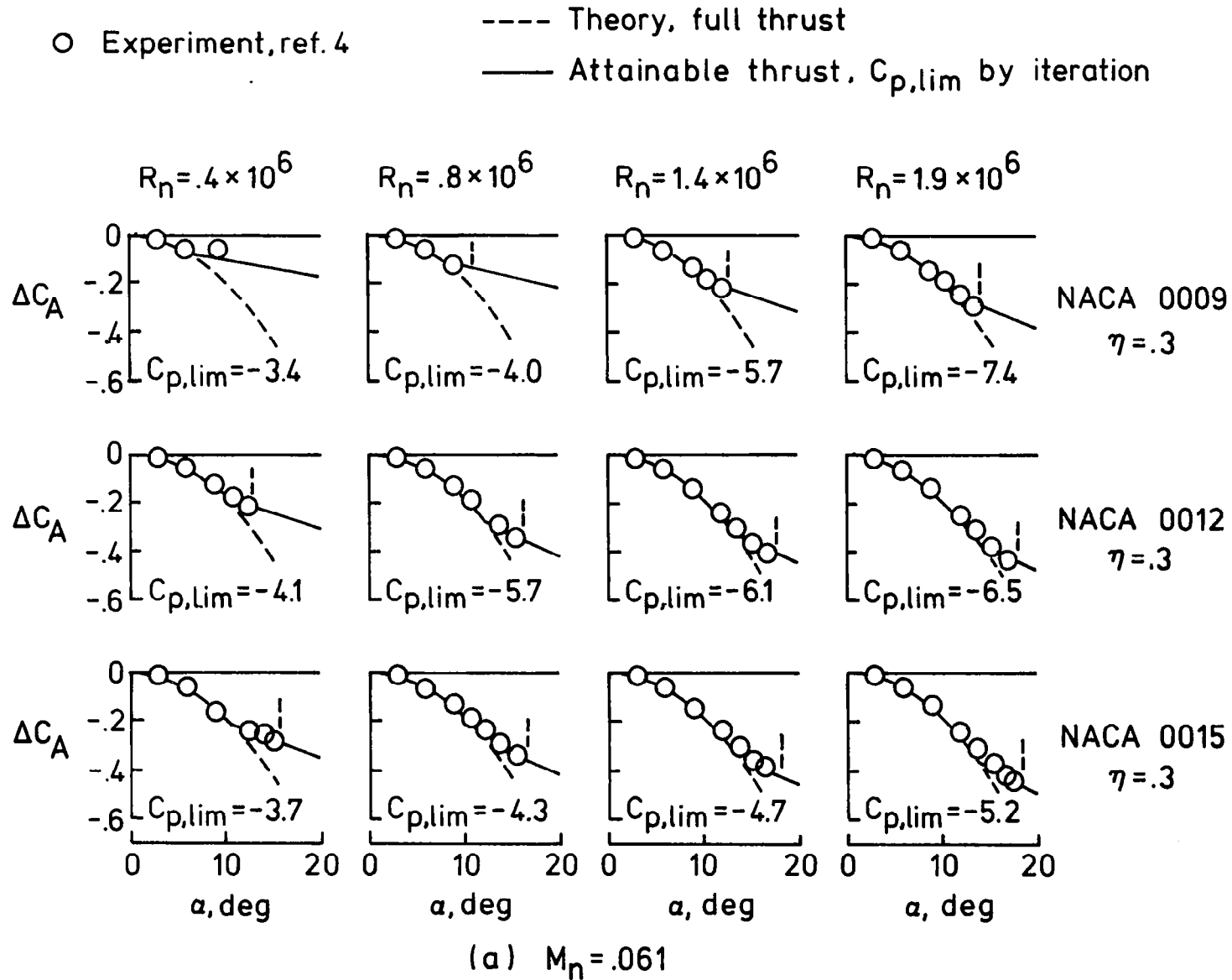
Figure 1.- Axial force characteristics of two-dimensional airfoils.

O Experiment, ref. 5   ---- Theory, full thrust

              ——— Attainable thrust, $C_{p,lim}$ by iteration

$M_n = .05, R_n = 1.1 \times 10^6$ $M_n = .11, R_n = 2.2 \times 10^6$ $M_n = .22, R_n = 4.1 \times 10^6$

$C_{p,lim} = -4.1$ $C_{p,lim} = -4.9$ $C_{p,lim} = -4.9$

NACA 0006

$\eta = .3$

$M_n = .03, R_n = .9 \times 10^6$ $M_n = .10, R_n = 1.8 \times 10^6$ $M_n = .17, R_n = 3.6 \times 10^6$

$C_{p,lim} = -4.7$ $C_{p,lim} = -5.9$ $C_{p,lim} = -6.2$

NACA 0008

$\eta = .3$

α, deg α, deg α, deg
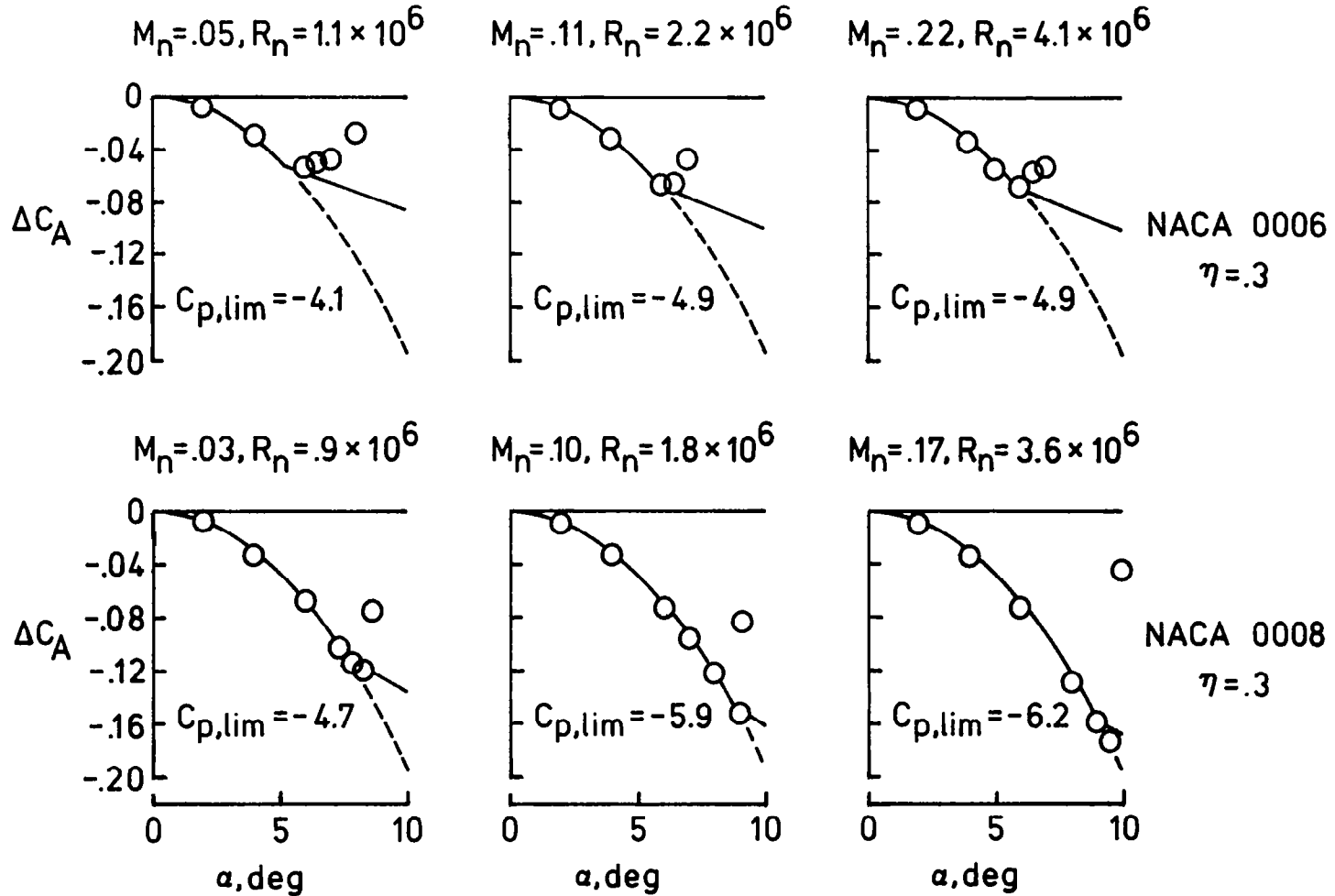
(b) M_n as specified

Figure 1.- Concluded.

○ Data from figure 1

--- Fairing

● Data points from fairing

Reference 4

$M_n = .061$

Reference 5

M_n as specified

(a) $M_n = .03$ to $.22$
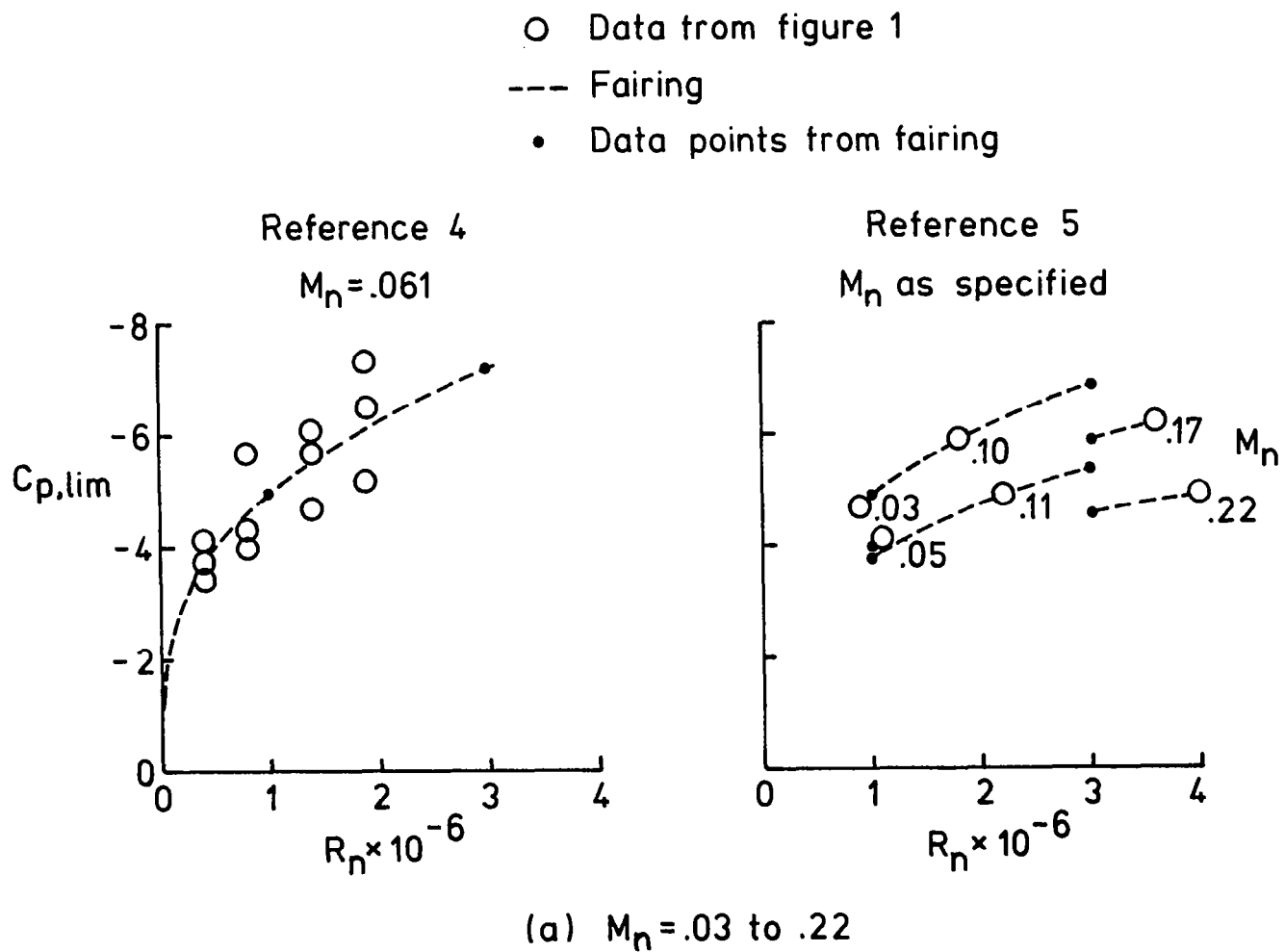
Figure 2.- Limiting pressure coefficient variation with Reynolds number.

O   Data from reference 3
--- Fairing
•   Data points from fairing
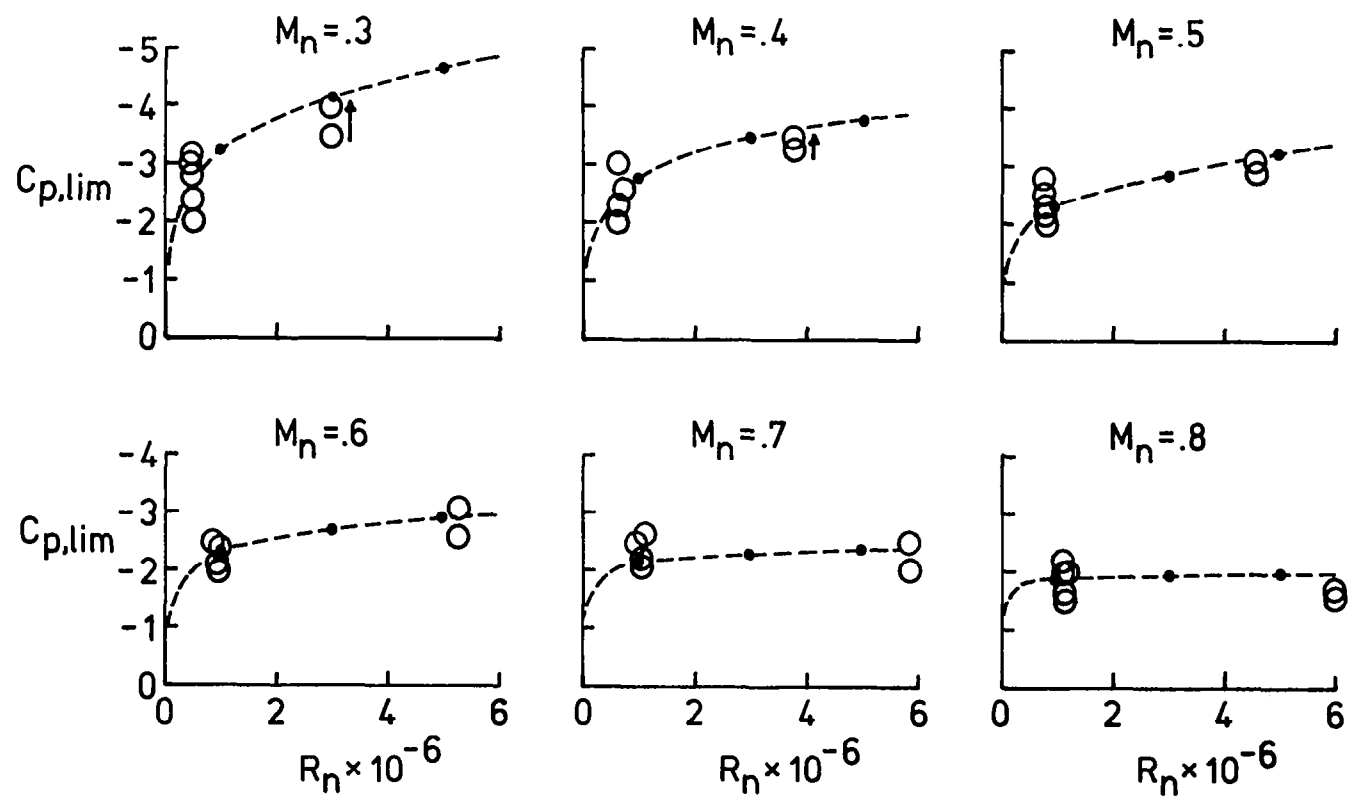
(b) $M_n = .3$ to .8

Figure 2.- Concluded.

Data from figure 2

$$R_n \times 10^{-6}$$

○   1

□   3

◇   5

—— Empirical equation

$$C_{p,lim} = \frac{-2}{\gamma M_n^2}\left[\frac{R_n \times 10^{-6}}{R_n \times 10^{-6} + 10^e}\right]^E$$

$$E = .05 + .35(1 - M_n)^2$$

$$e = 4 - 3M_n + 4(1 - M_n)^{15}$$
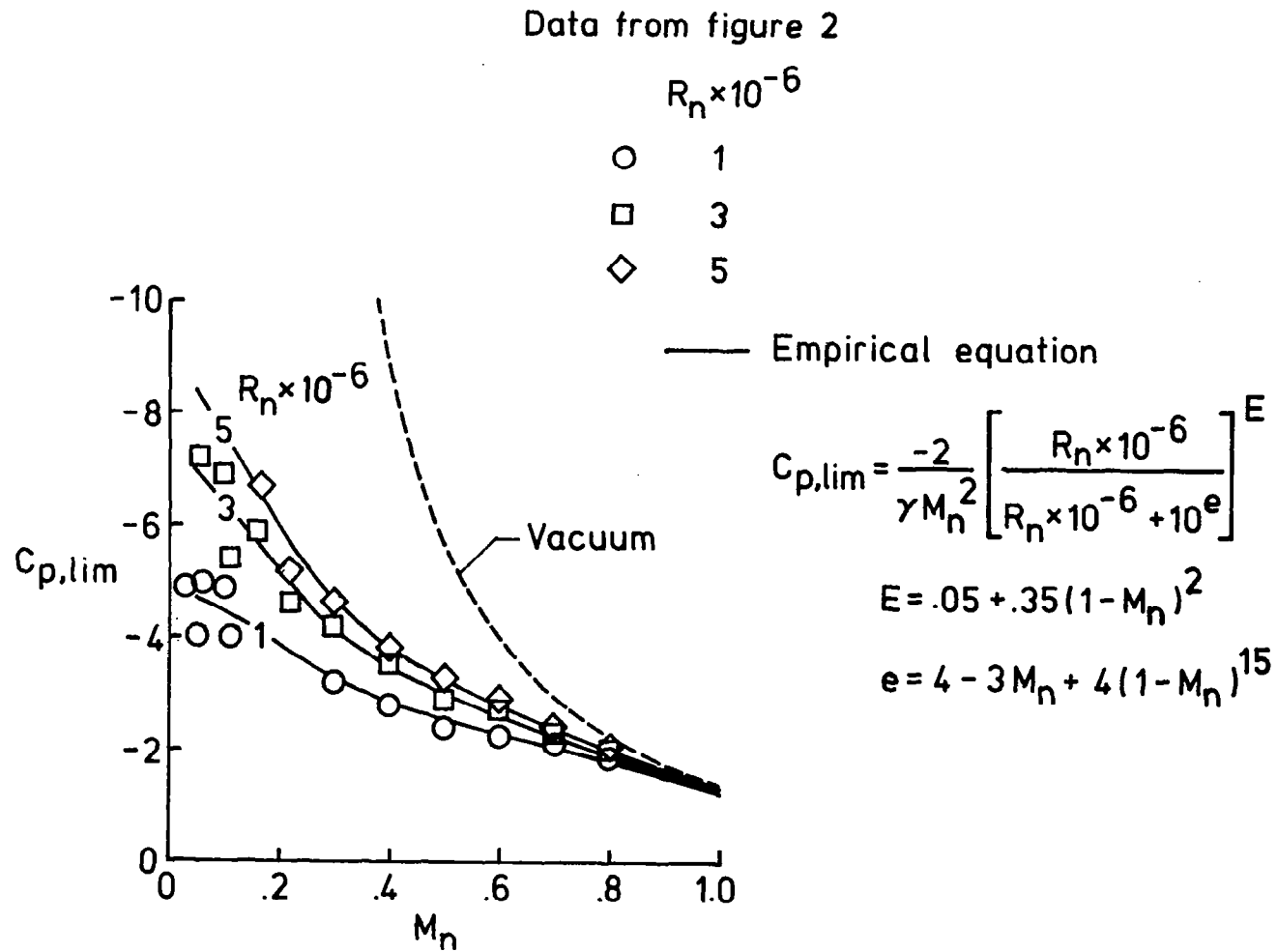
Figure 3.- Limiting pressure coefficient variation with Mach number.
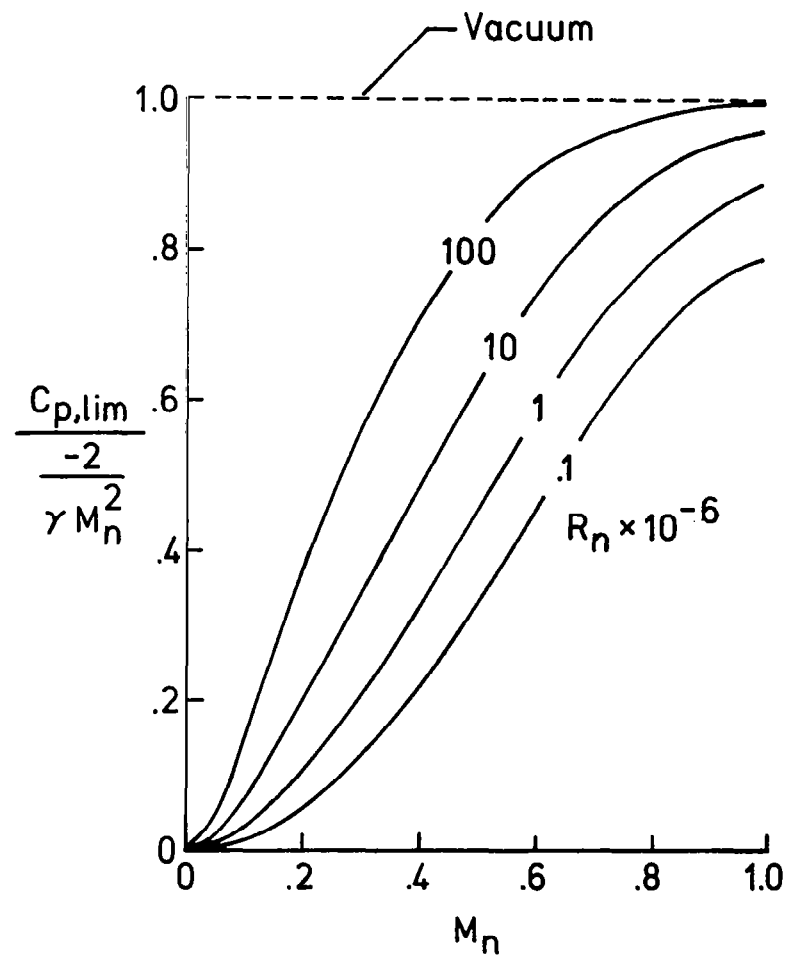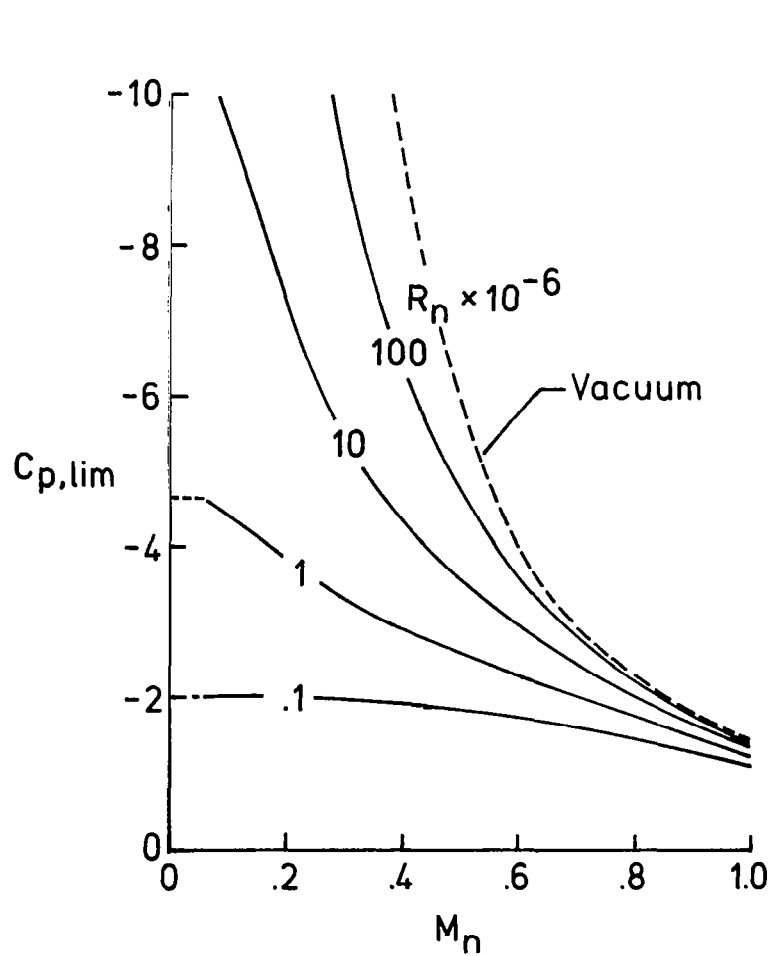
Figure 4.- Limiting pressure coefficient as given by the empirical formula.
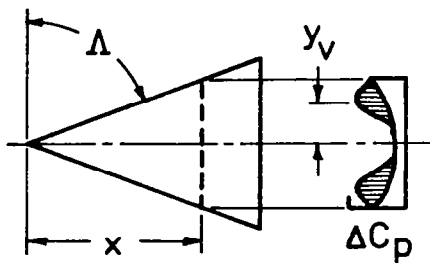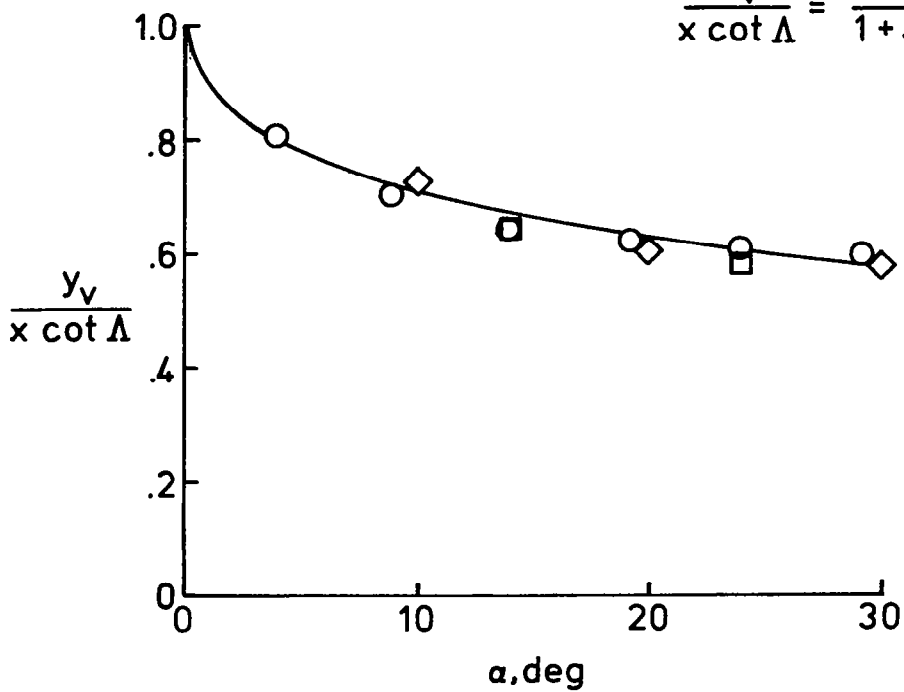
Figure 5.- Location of center of vortex pressure field as given by experimental data.
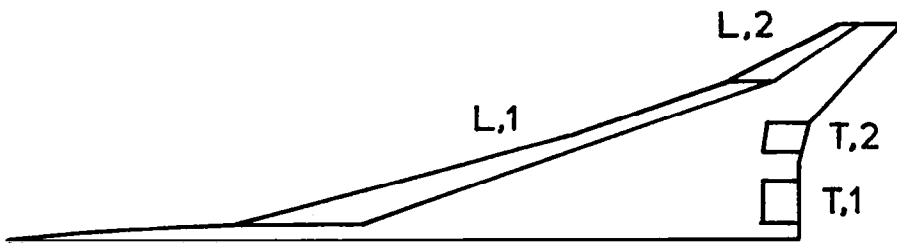
$$\delta_{T,n} = \delta_{T,1,n} = \delta_{T,2,n}$$

$$\delta_{L,n} = \delta_{L,1,n} = \delta_{L,2,n}$$
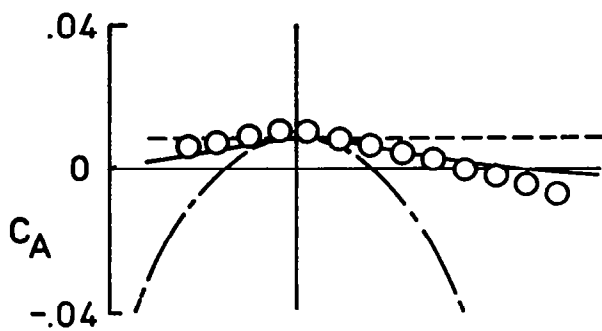
O Experiment

Theory

------- No thrust

—·— Full thrust
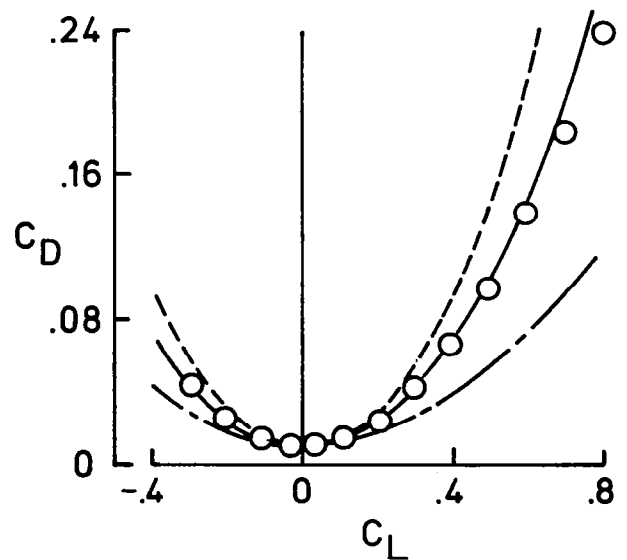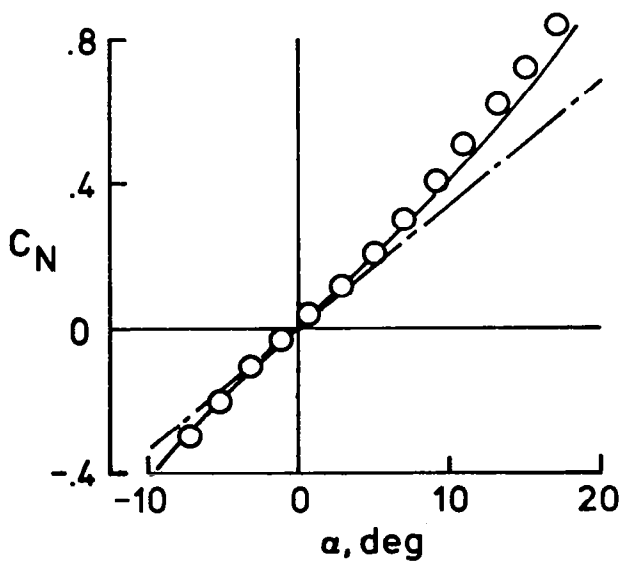
——— Present method

(a) $\delta_{T,n} = 0°$, $\delta_{L,n} = 0°$

Figure 6.- Correlation of program data with experimental
data for an arrow wing configuration.
M = 0.28, R = 5.75 x 10^6

$$\delta_{T,n} = \delta_{T,1,n} = \delta_{T,2,n}$$

$$\delta_{L,n} = \delta_{L,1,n} = \delta_{L,2,n}$$

O Experiment

Theory

------- No thrust

—·—· Full thrust
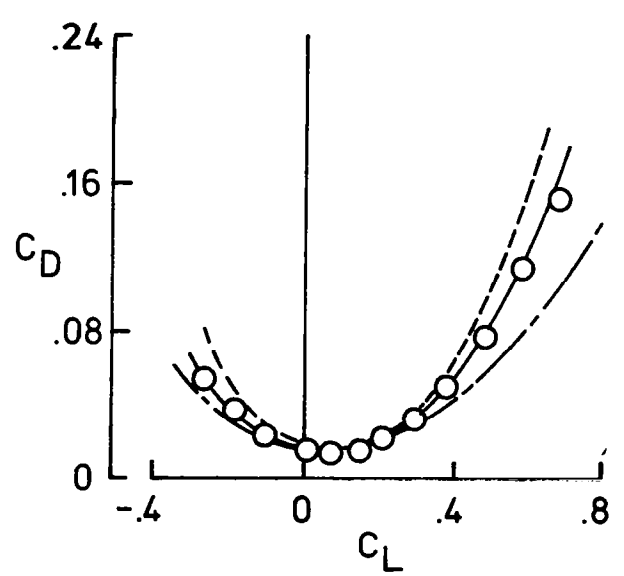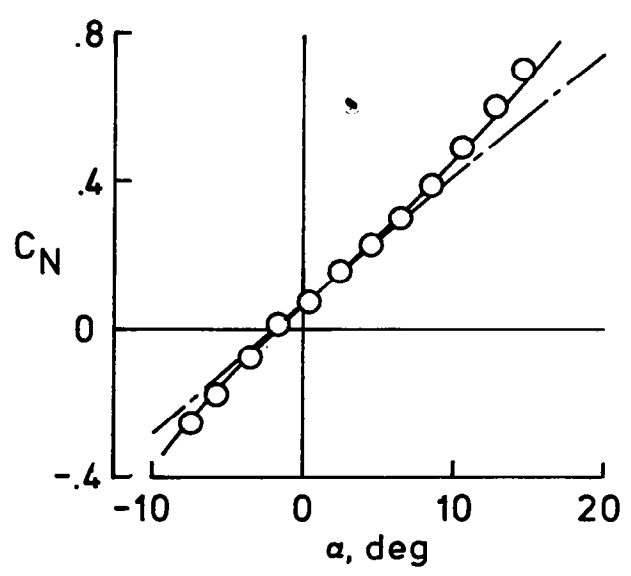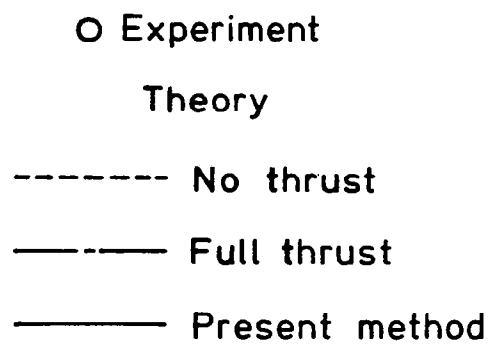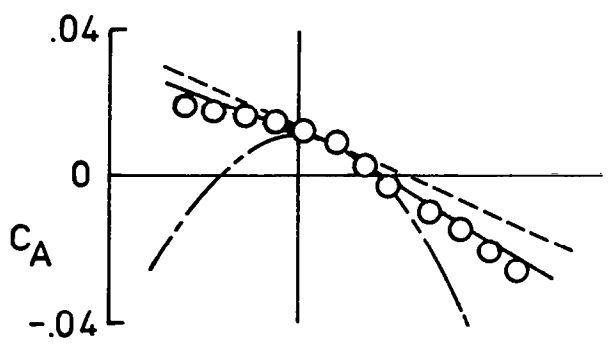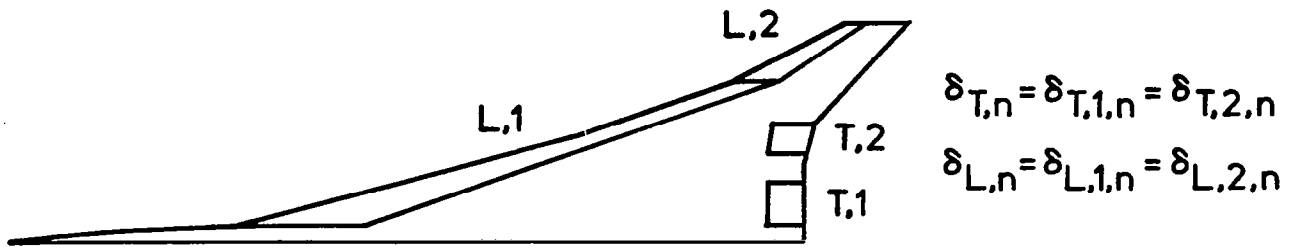
——— Present method

(b) $\delta_{T,n} = 10°$, $\delta_{L,n} = 20°$

Figure 6.- Continued.
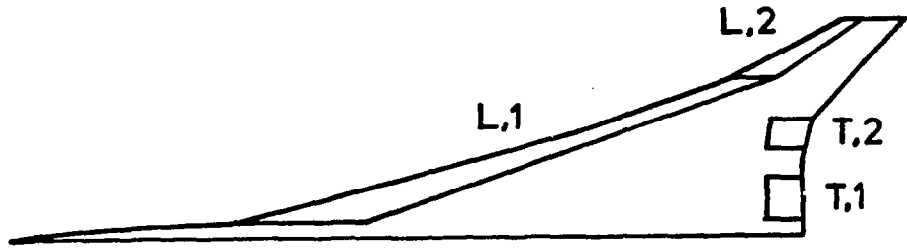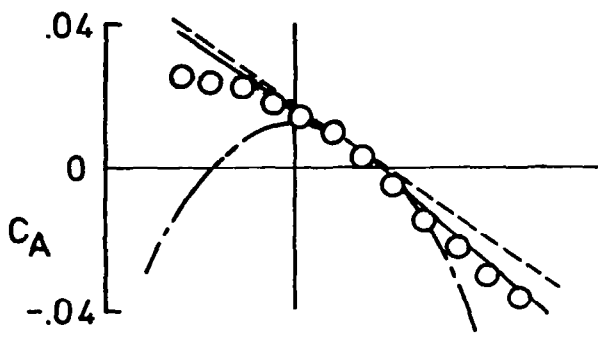
$$\delta_{T,n} = \delta_{T,1,n} = \delta_{T,2,n}$$
$$\delta_{L,n} = \delta_{L,1,n} = \delta_{L,2,n}$$

O Experiment

Theory

------- No thrust

—·— Full thrust
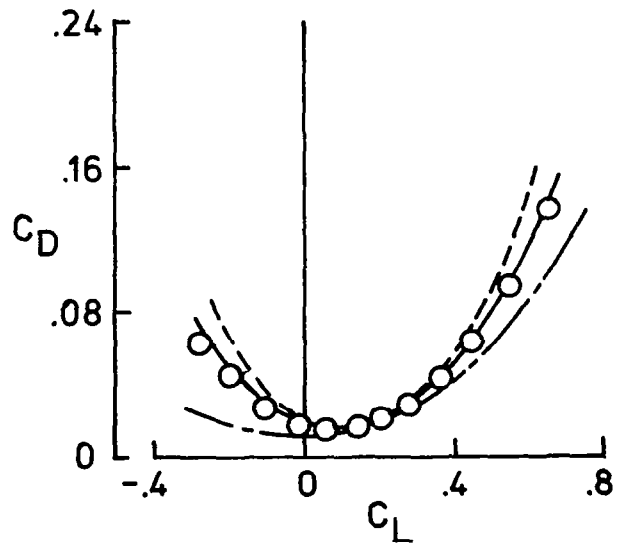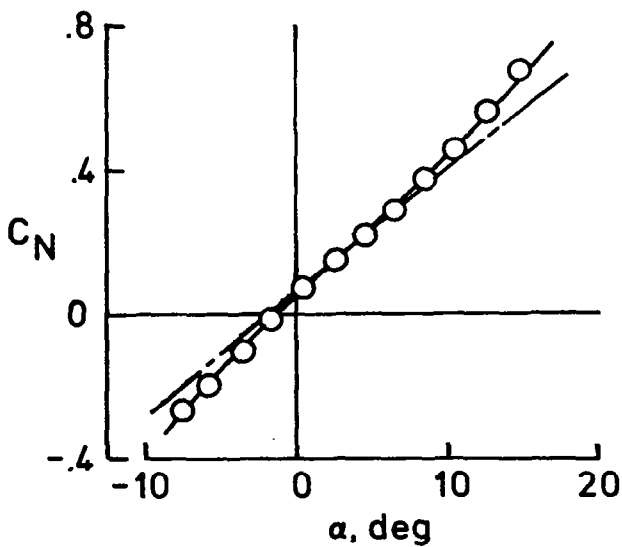
——— Present method

(c) $\delta_{T,n} = 10°$, $\delta_{L,n} = 30°$

Figure 6.- Continued.
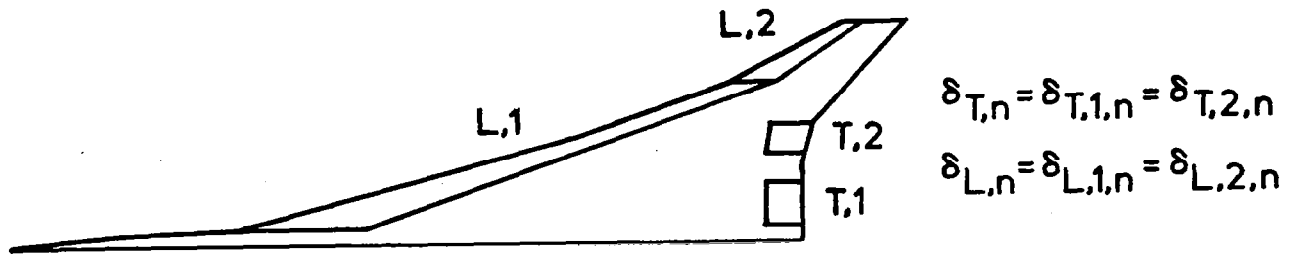
$$\delta_{T,n} = \delta_{T,1,n} = \delta_{T,2,n}$$
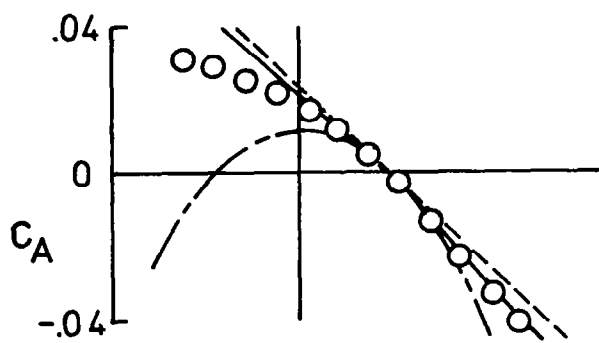
$$\delta_{L,n} = \delta_{L,1,n} = \delta_{L,2,n}$$

O Experiment

Theory

------ No thrust

—·—· Full thrust
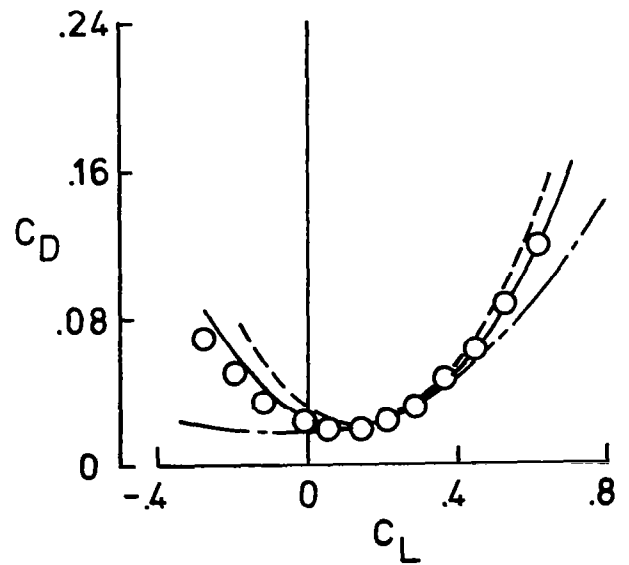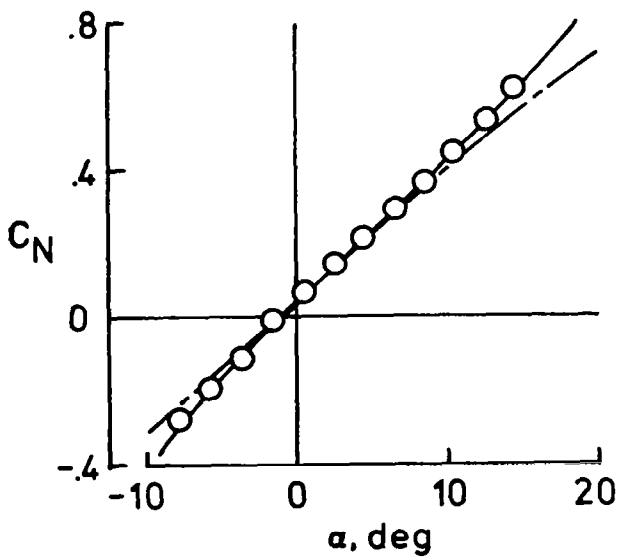
——— Present method

(d) $\delta_{T,n} = 10°, \ \delta_{L,n} = 40°$

Figure 6.- Continued.
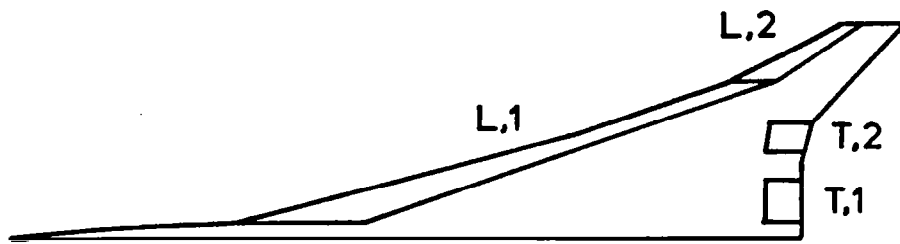
$$\delta_{T,n} = \delta_{T,1,n} = \delta_{T,2,n}$$
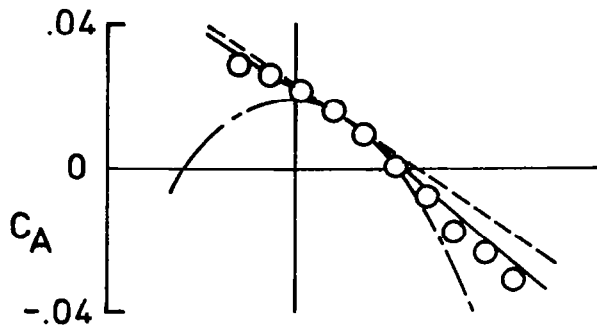
$$\delta_{L,n} = \delta_{L,1,n} = \delta_{L,2,n}$$

O Experiment

Theory

------- No thrust

—·— Full thrust

——— Present method

(e) $\delta_{T,n} = 20°$, $\delta_{L,n} = 30°$

Figure 6.- Continued.

$\delta_{T,n} = \delta_{T,1,n} = \delta_{T,2,n}$
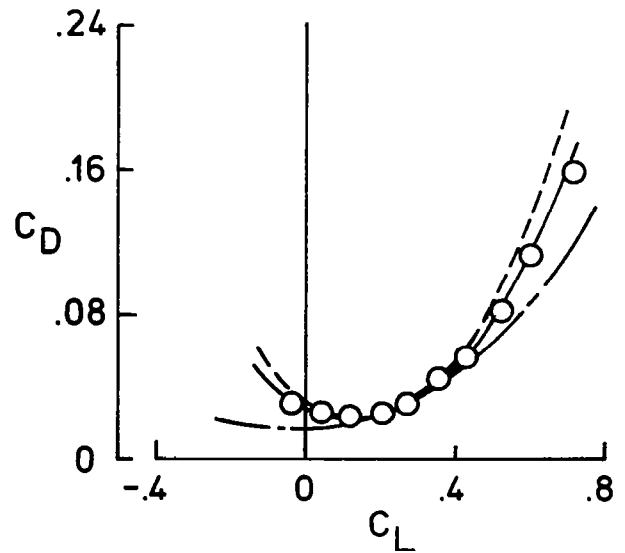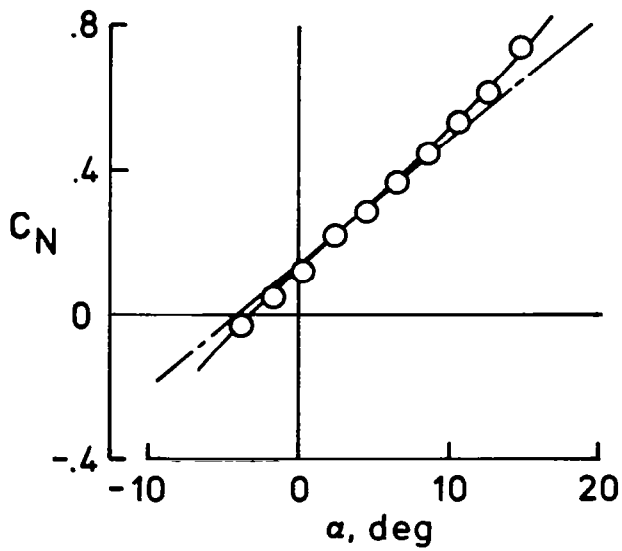
$\delta_{L,n} = \delta_{L,1,n} = \delta_{L,2,n}$

O Experiment

Theory
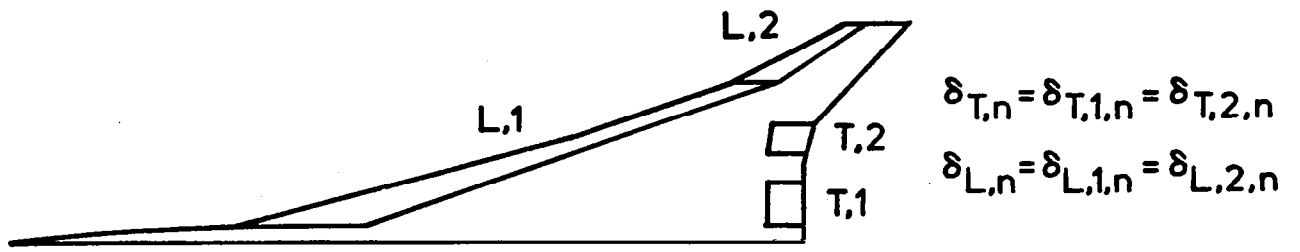
------ No thrust

—·— Full thrust
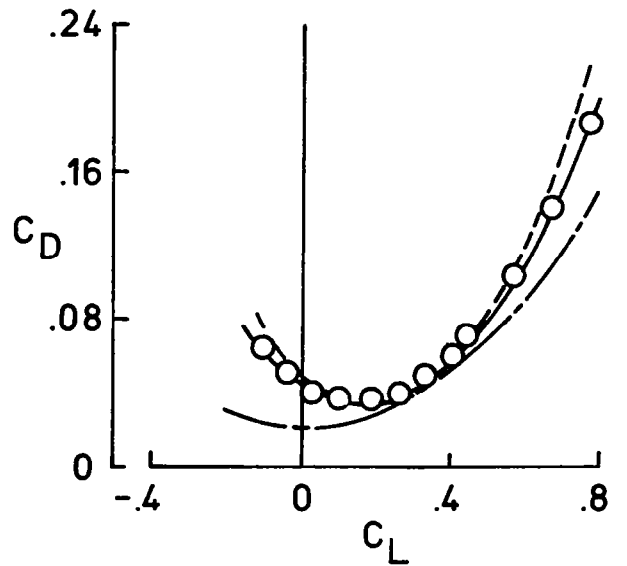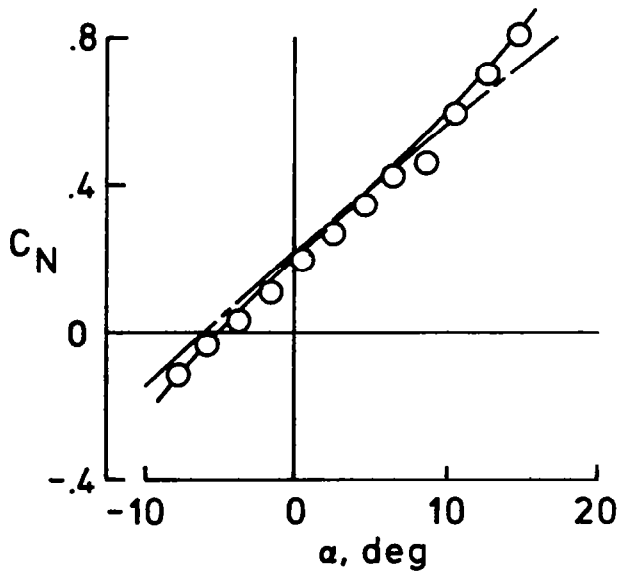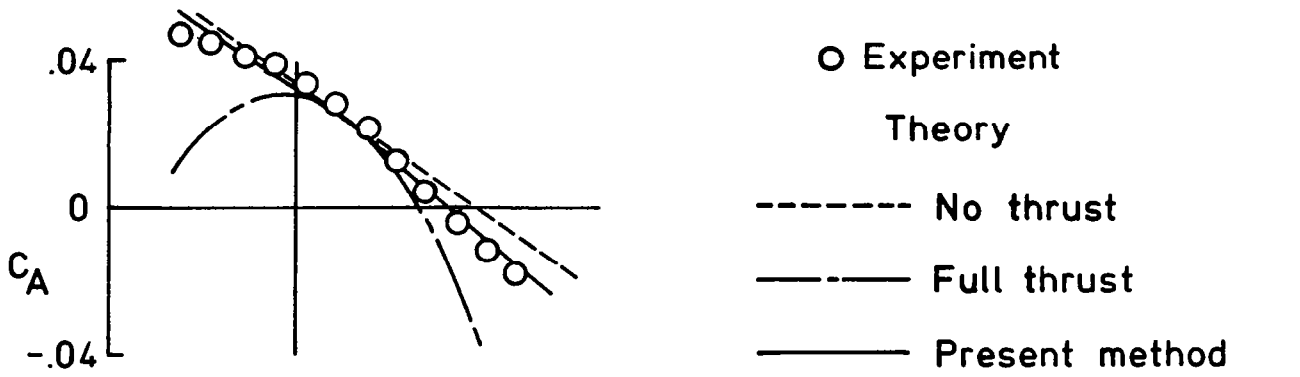
—— Present method

(f) $\delta_{T,n} = 30°$, $\delta_{L,n} = 30°$

Figure 6.- Continued.

$$\delta_{T,n} = \delta_{T,1,n} = \delta_{T,2,n}$$

$$\delta_{L,n} = \delta_{L,1,n} = \delta_{L,2,n}$$
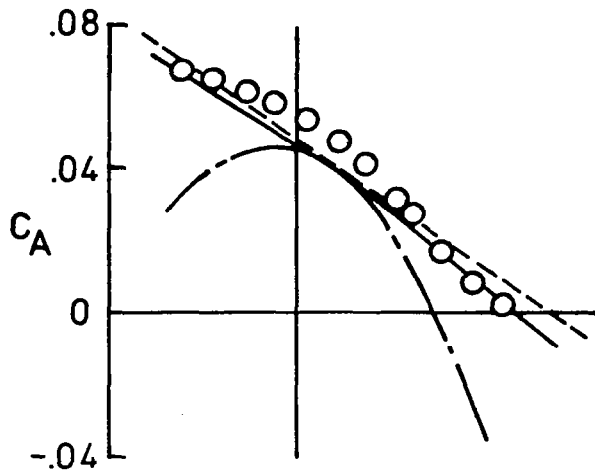
O Experiment

Theory

------- No thrust

--·-- Full thrust

——— Present method
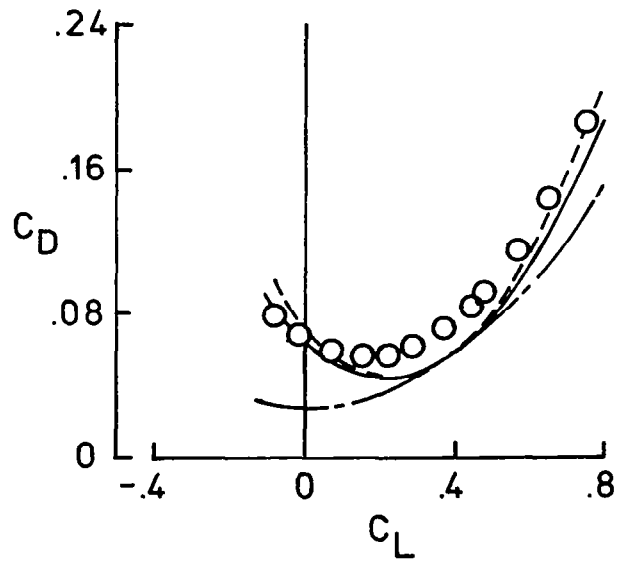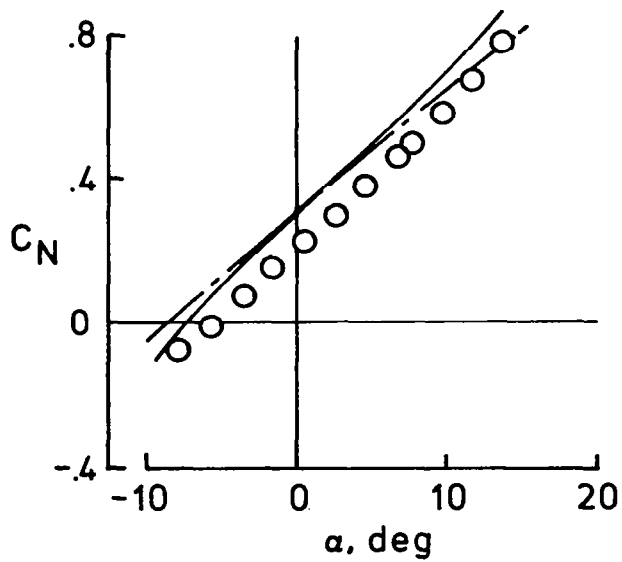
(g) $\delta_{T,n} = 40°$, $\delta_{L,n} = 30°$

Figure 6.- Concluded.

59

O Experiment

Theory

------- No thrust

—·— Full thrust

——— Present method
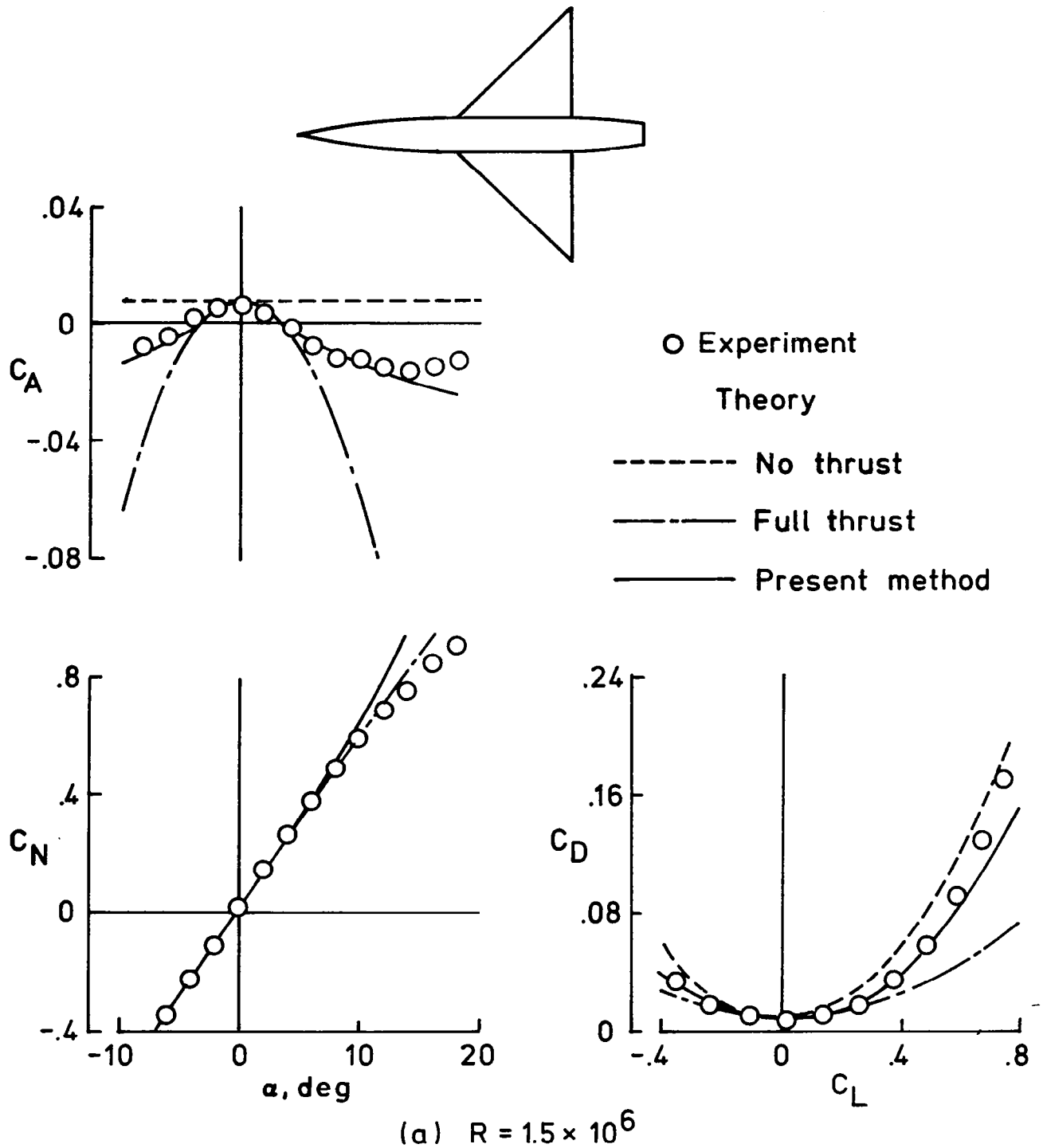
(a)   R = 1.5 × 10^6

Figure 7.- Correlation of program data with experimental
data for a flat delta wing configuration.
M = 0.25.

O Experiment

Theory

------ No thrust

—·— Full thrust
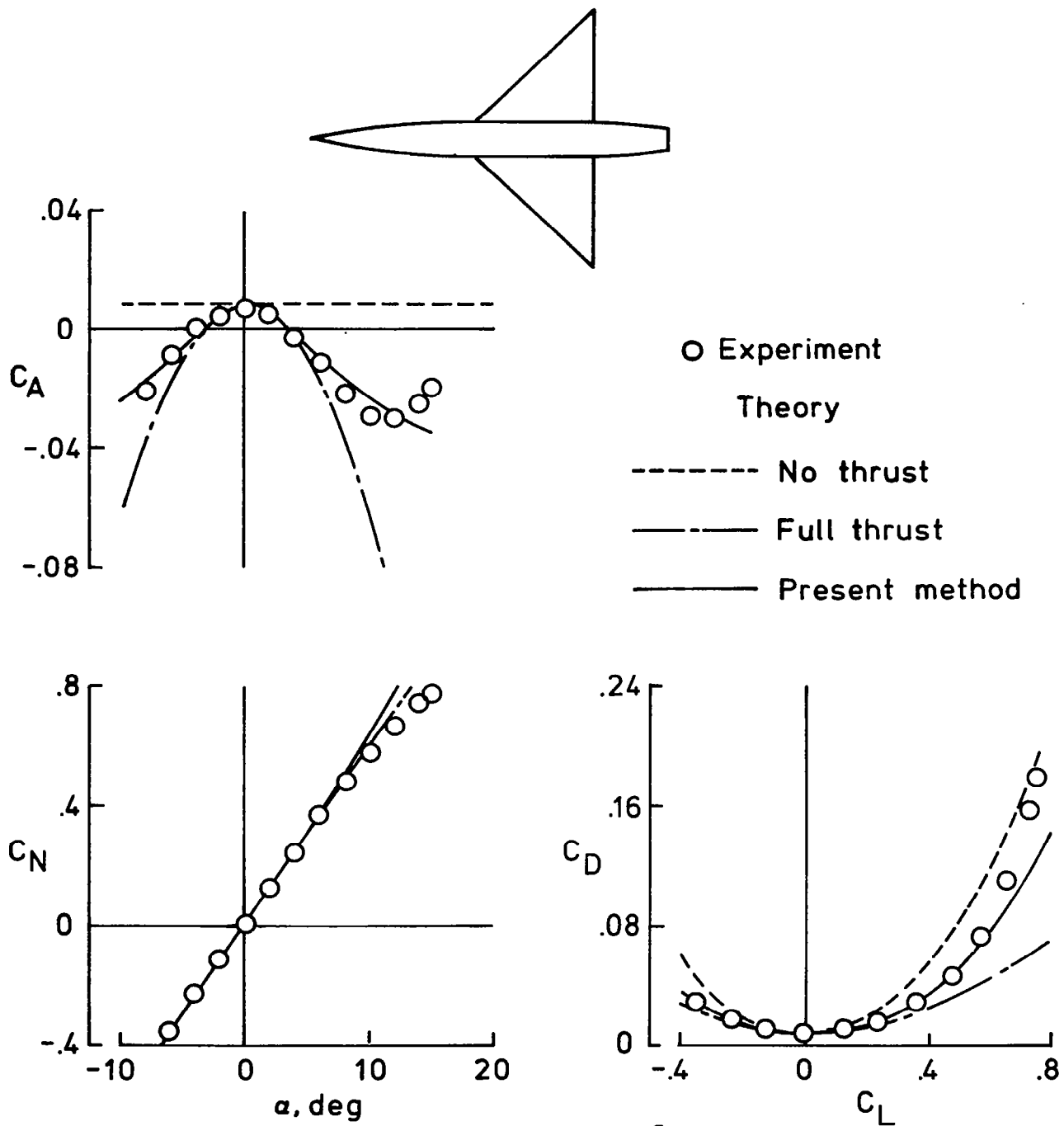
——— Present method

(b) R = 8.0 × 10^6

Figure 7.- Concluded.
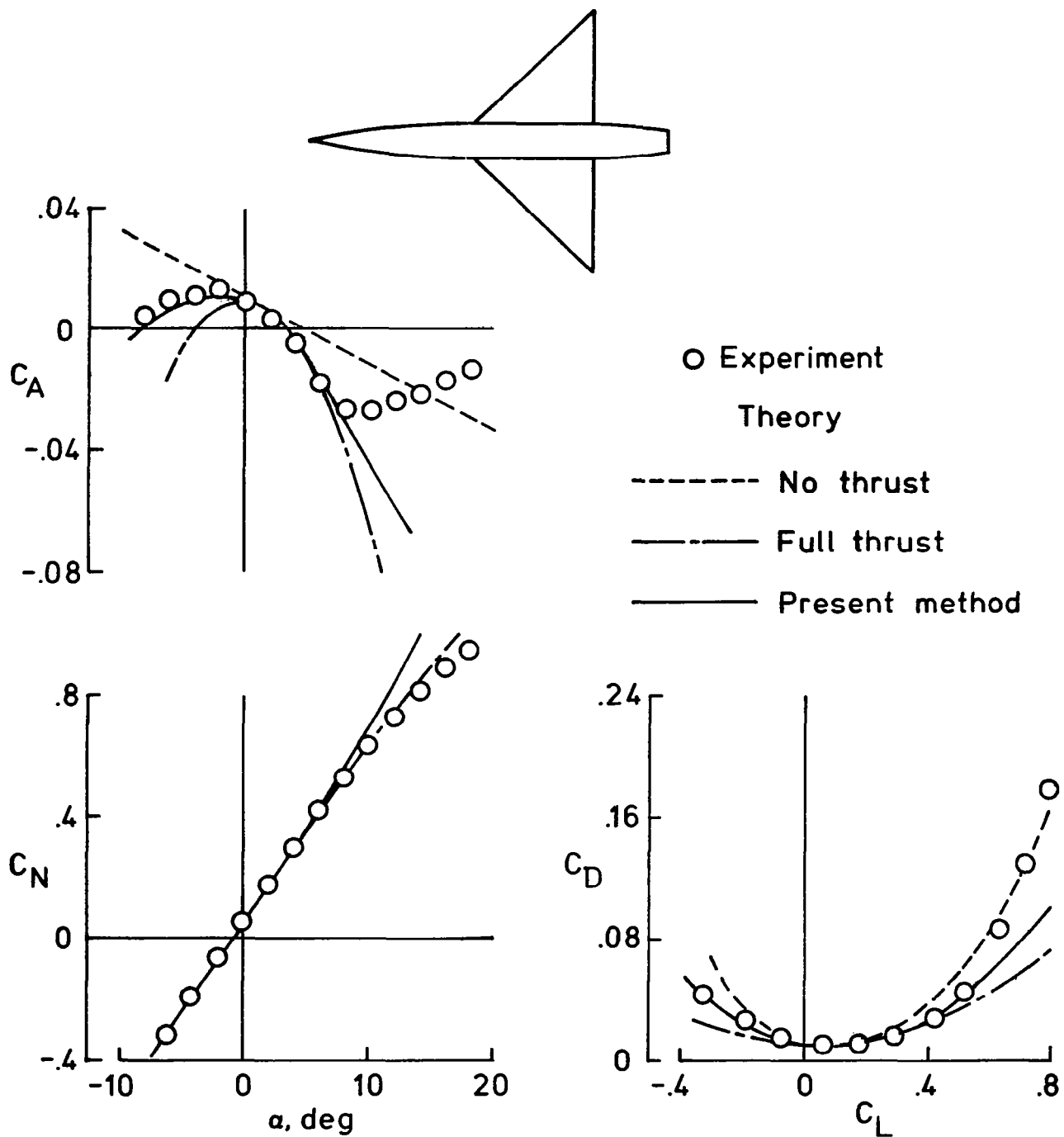
Figure 8.- Correlation of program data with experimental data for a twisted and cambered delta wing configuration. M = 0.25.

O Experiment

Theory

------- No thrust

—·—— Full thrust
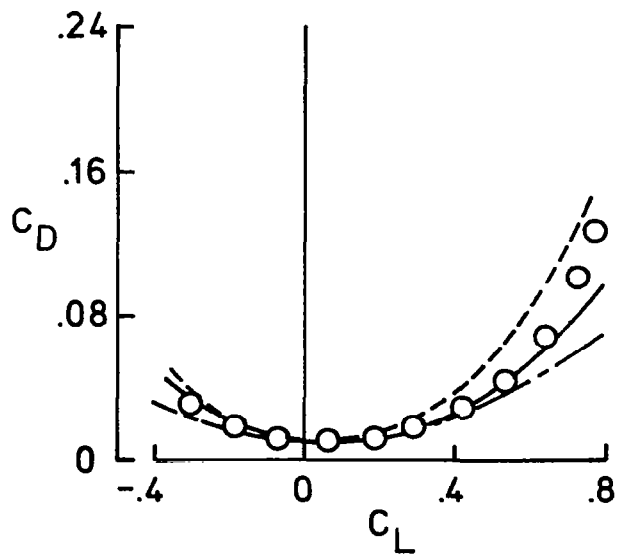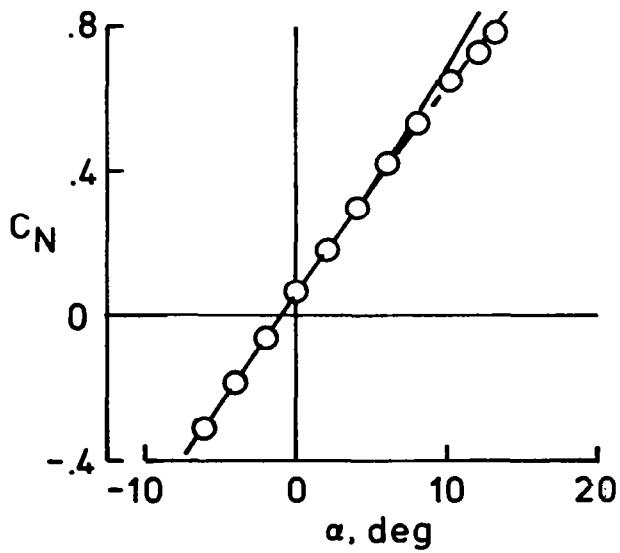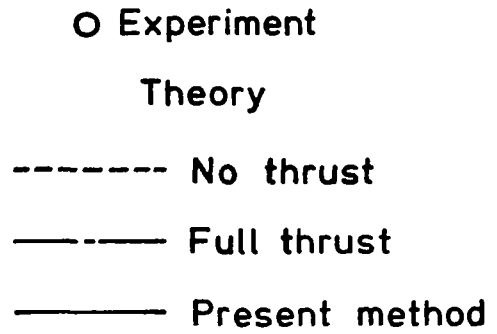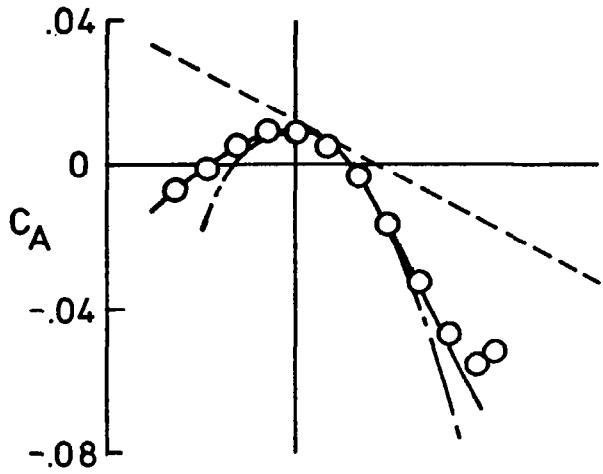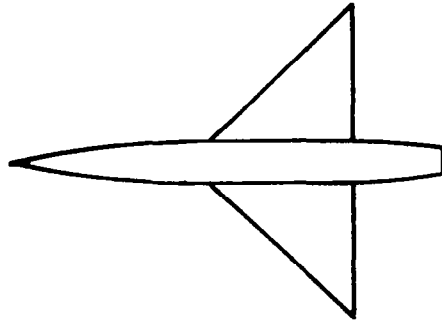
——— Present method

(b) R = 8.0 × 10^6

Figure 8.- Concluded.
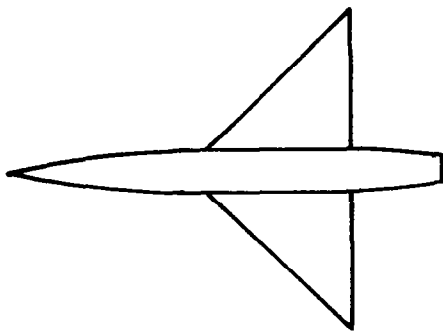
63
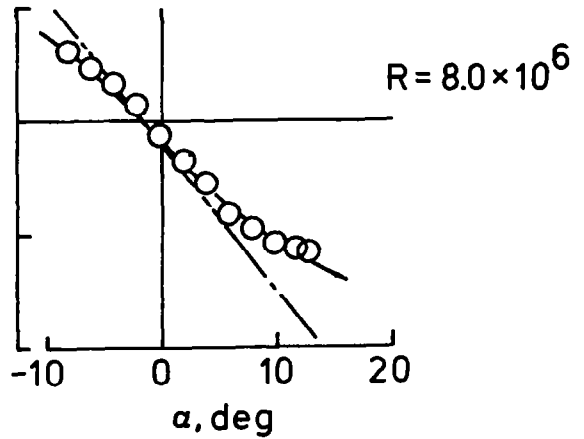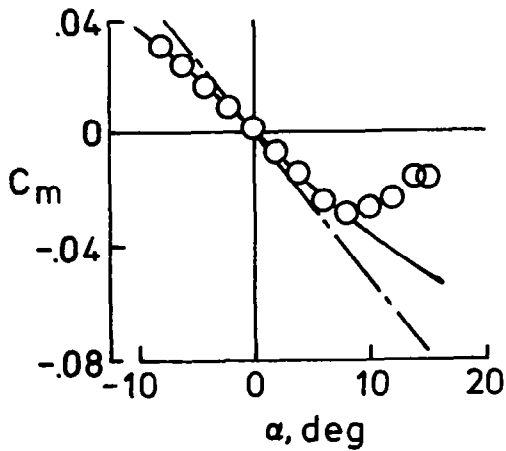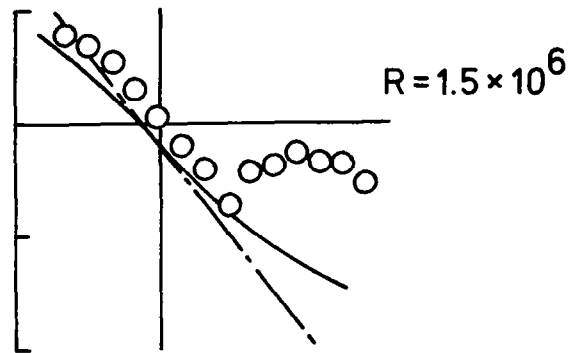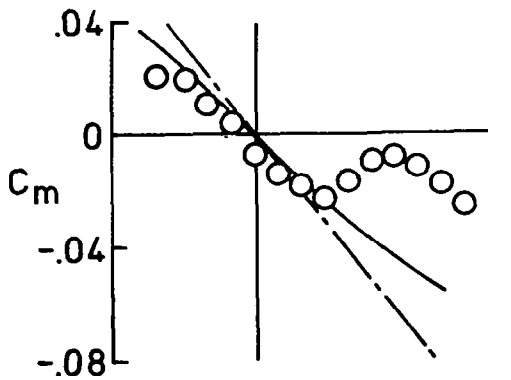
Figure 9.- An example of the effect of Reynolds number
on pitching moment.
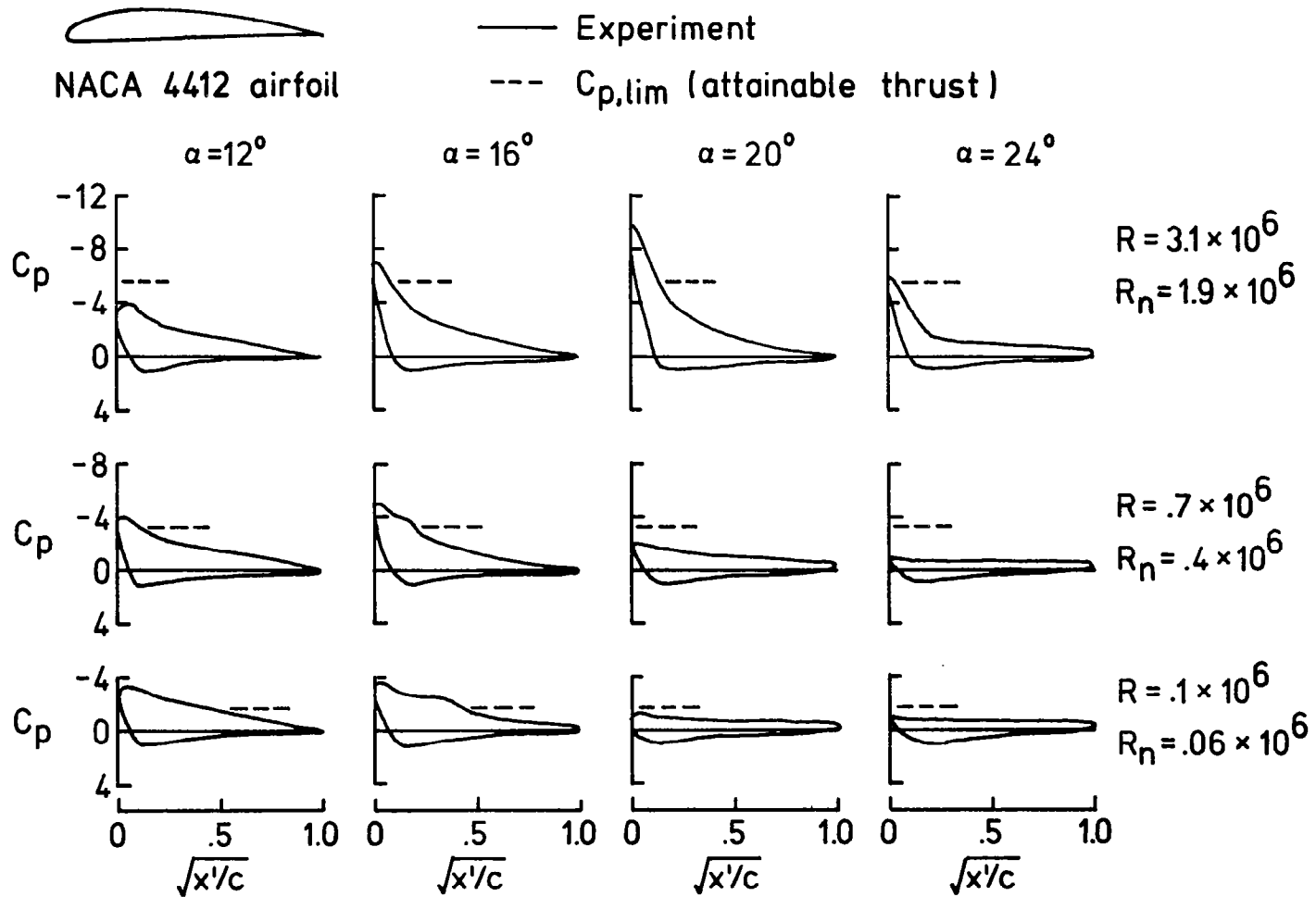
Figure 10.- Pressure distribution on an airfoil at
three Reynolds numbers. M = 0.61.
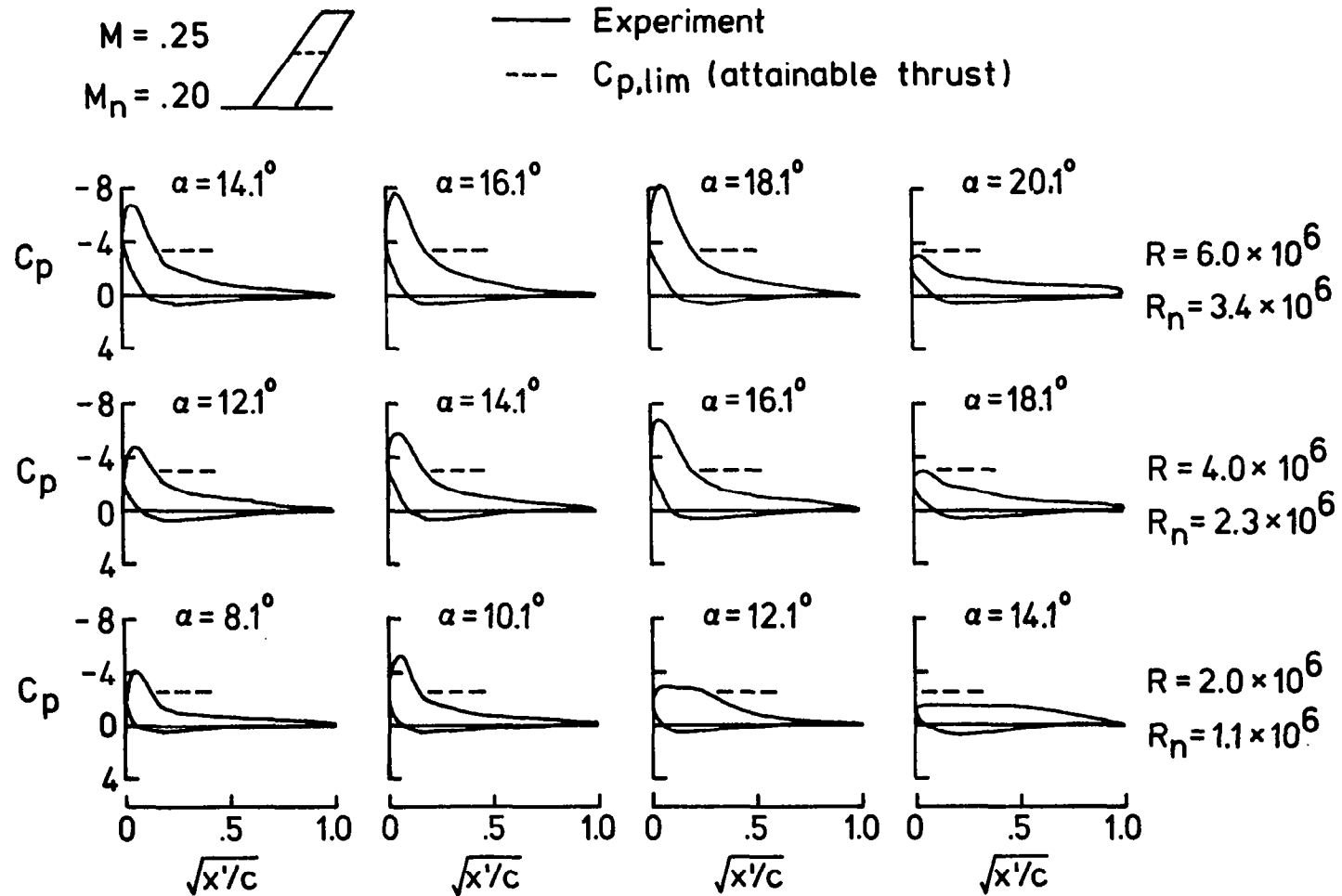
Figure 11.- Pressure distribution on a semispan swept wing at three Reynolds numbers. M = 0.25.
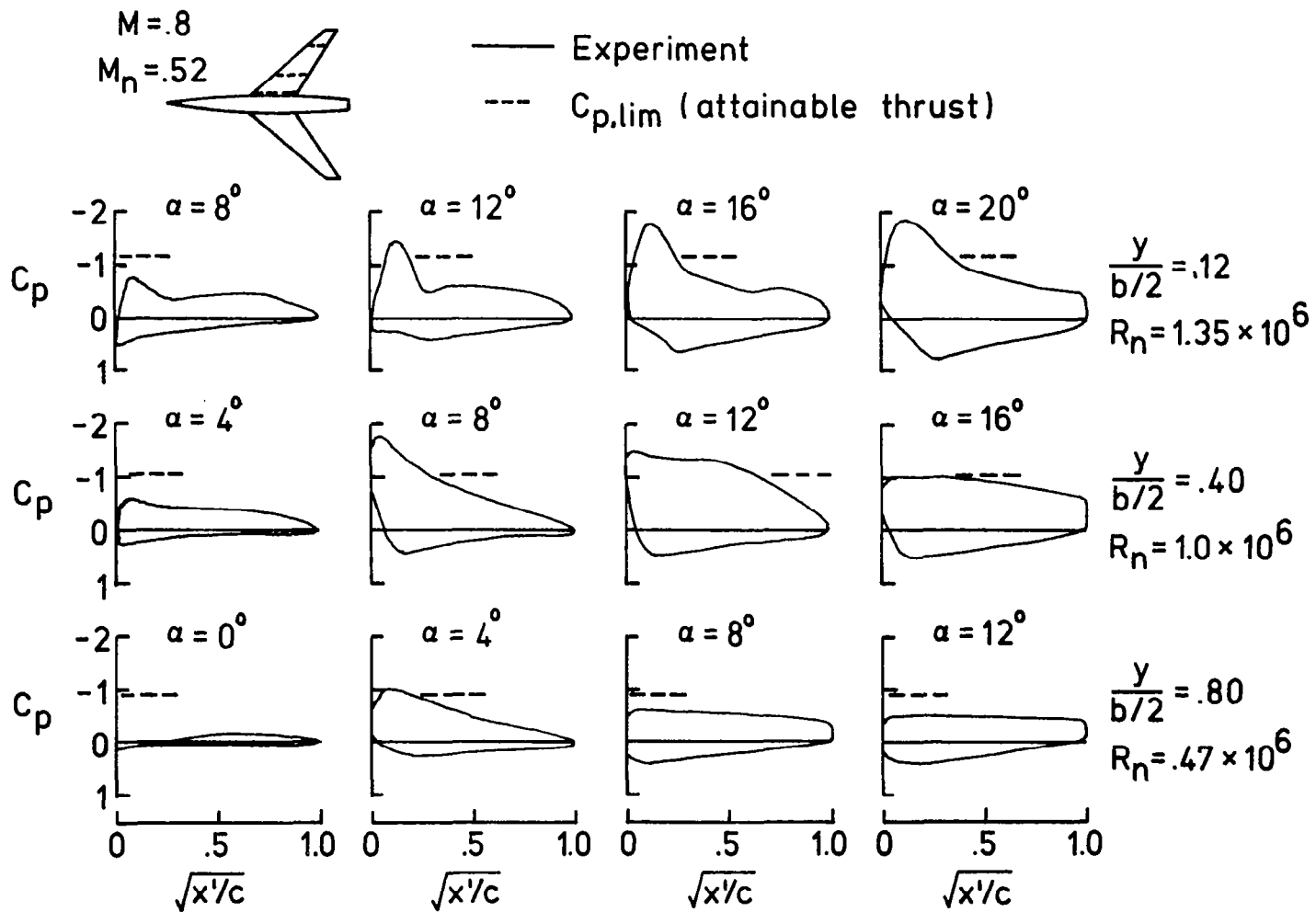
Figure 12.- Pressure distribution on a wing-body combination at three span
stations. M = 0.8.
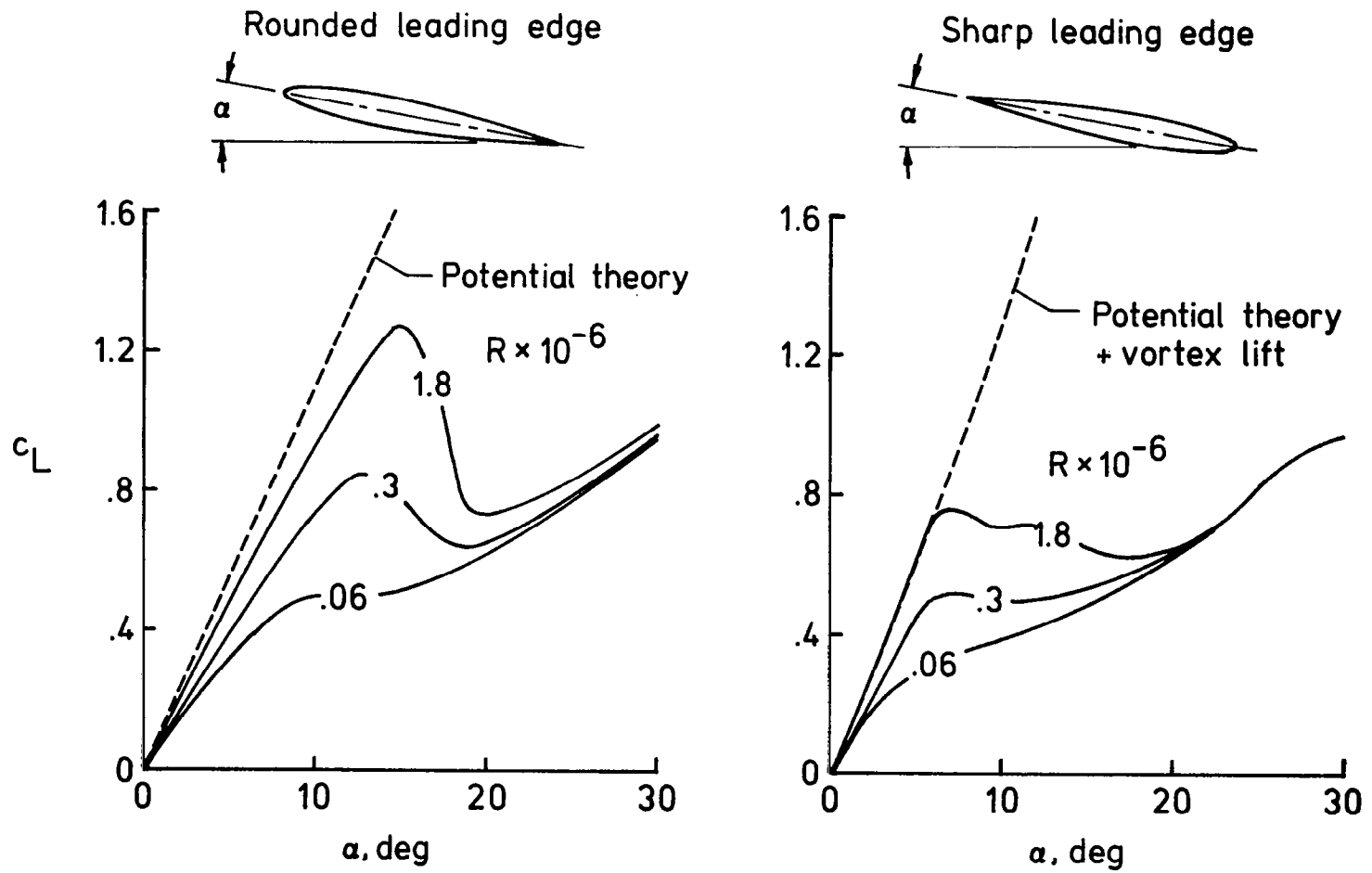
Figure 13.- Effect of Reynolds number on lift coefficient of wind energy airfoil.
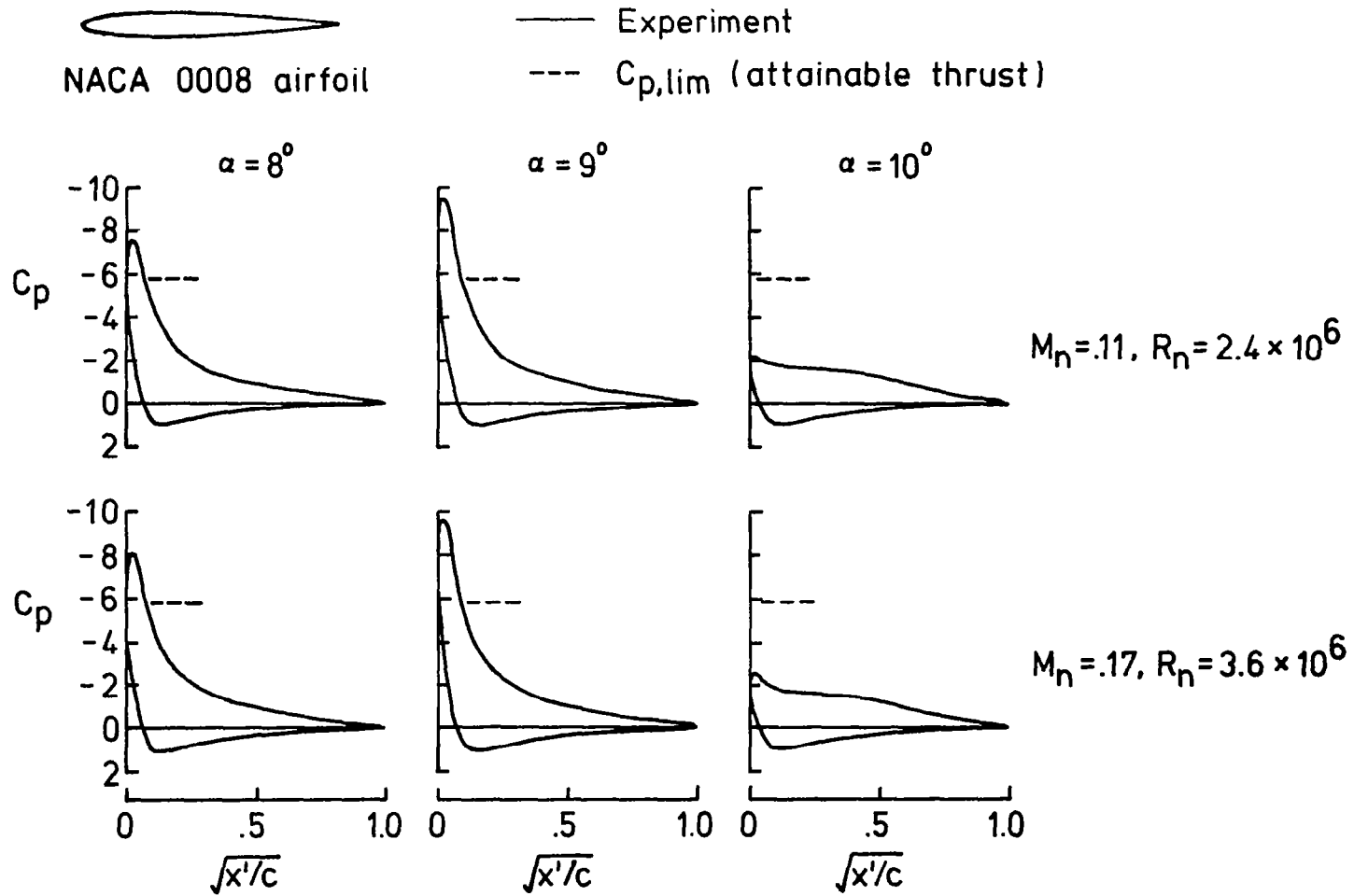
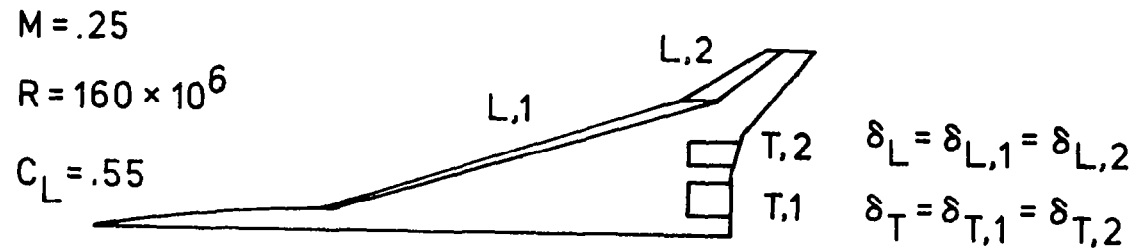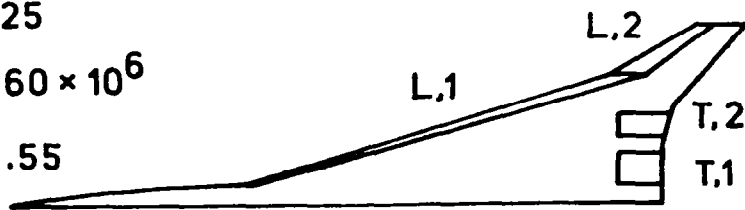Figure 14.- Illustration of a precipitous change in pressure distribution.

$M = .25$

$R = 160 \times 10^6$

$C_L = .55$

L,2

L,1

T,2

T,1

$\delta_L = \delta_{L,1} = \delta_{L,2}$
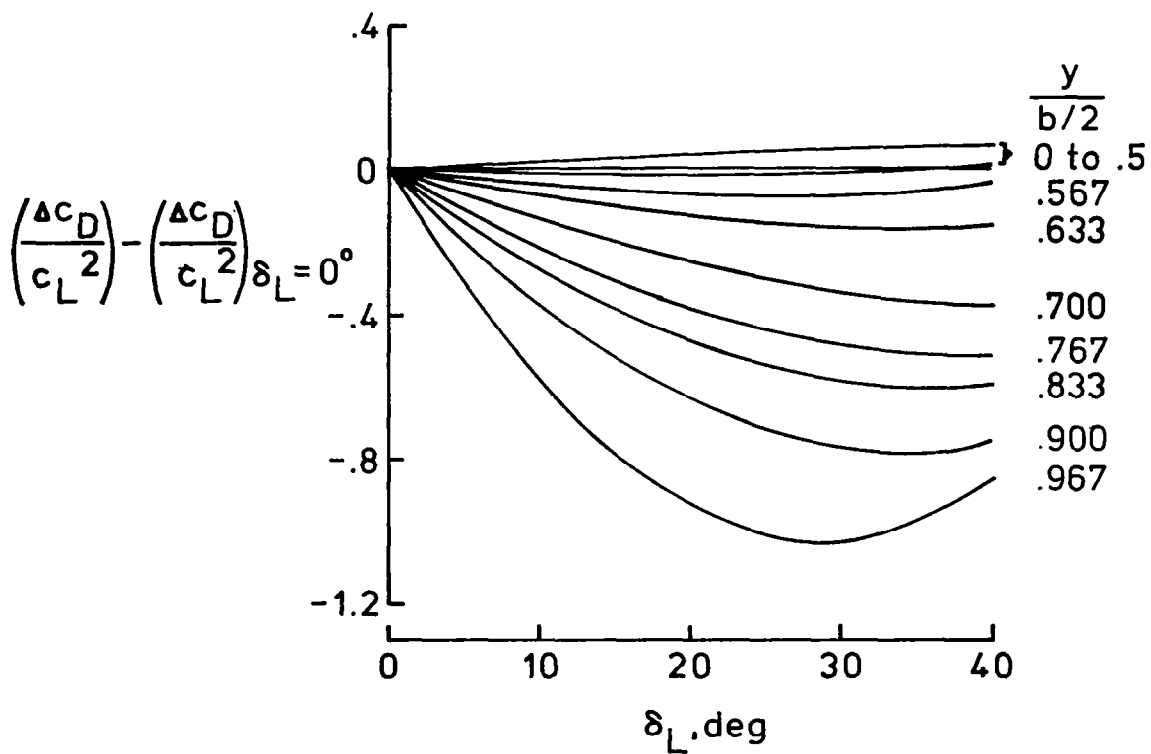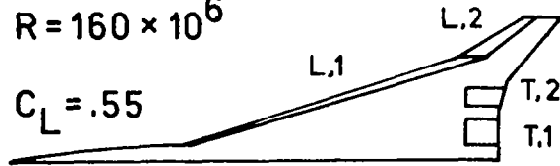
$\delta_T = \delta_{T,1} = \delta_{T,2}$

α, deg

.70 Suction parameter, S_s

δ_L, deg

δ_T, deg
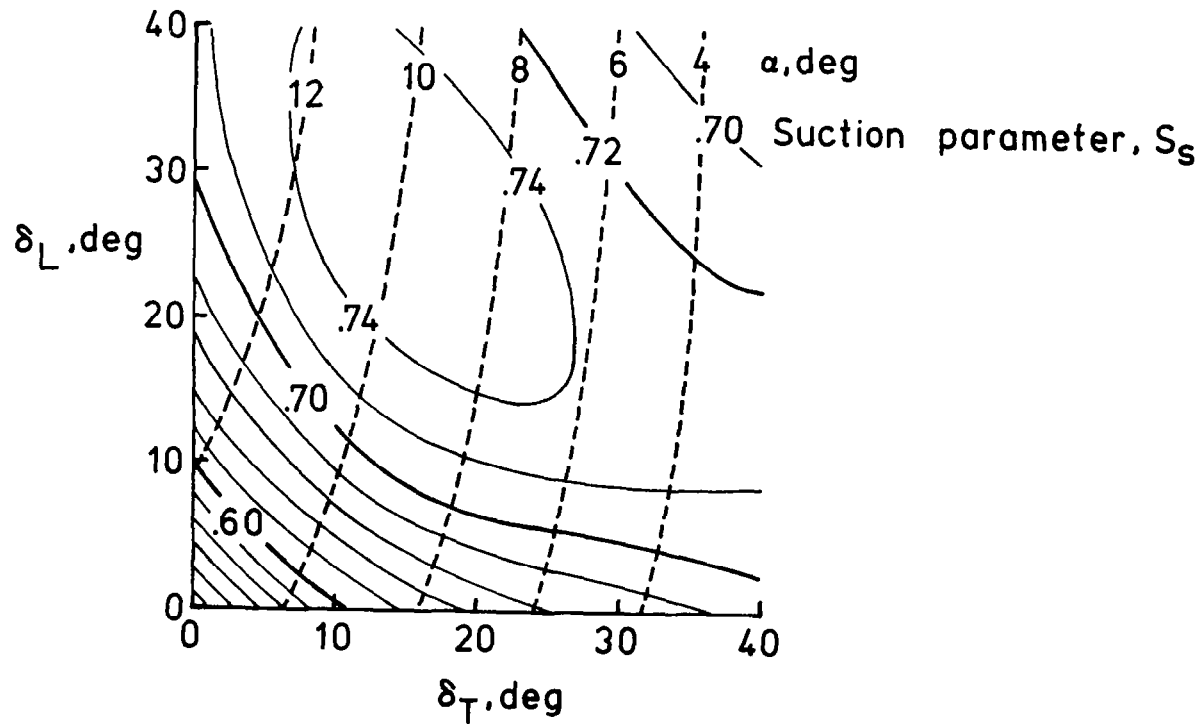
Figure 15.- Flap deflection optimization data for a candidate flap system.

Figure 16.- Variation of section drag-due-to-lift
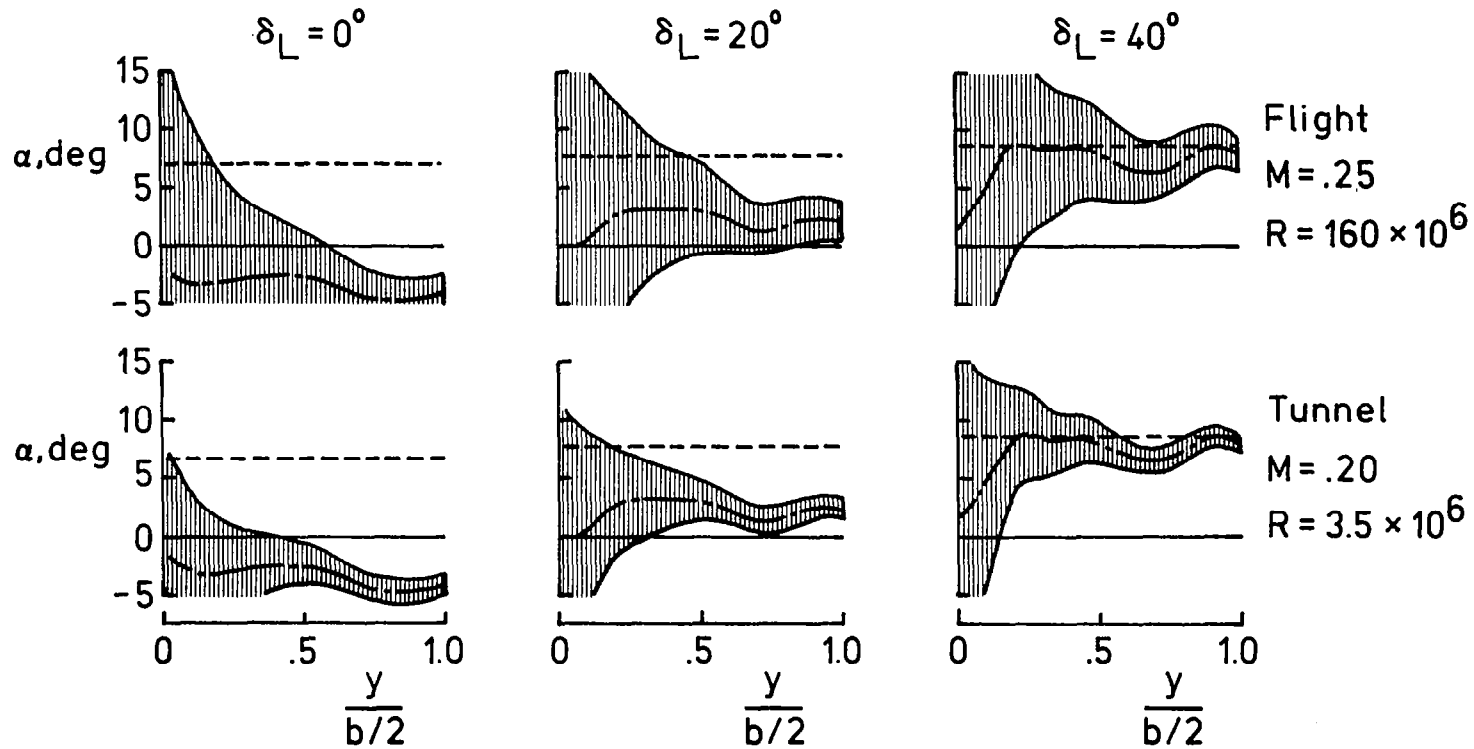factors with deflection of candidate
leading-edge flaps.

Figure 17.- Program estimate of the range of full thrust for the candidate flap system.

1. Report No. NASA CR-3675	2. Government Accession No.	3. Recipient's Catalog No.
4. Title and Subtitle AN AERODYNAMIC ANALYSIS COMPUTER PROGRAM AND DESIGN NOTES FOR LOW SPEED WING FLAP SYSTEMS		5. Report Date March 1983
		6. Performing Organization Code
7. Author(s) Harry W. Carlson and Kenneth B. Walkley		8. Performing Organization Report No.
		10. Work Unit No.
9. Performing Organization Name and Address Kentron International, Inc. Kentron Technical Center Hampton, VA 23666		11. Contract or Grant No. NAS1-16000
		13. Type of Report and Period Covered Contractor Report
12. Sponsoring Agency Name and Address National Aeronautics and Space Administration Washington, DC 20546		14. Sponsoring Agency Code 505-43-23-10

15. Supplementary Notes

Langley Technical Monitor: Barrett L. Shrout
Final Report

16. Abstract

This report describes the expanded capabilities for analysis and design of low speed flap systems afforded by recent modifications of an existing computer program. The program provides for the simultaneous analysis of up to 25 pairs of leading-edge and trailing-edge flap deflection schedules. Among other new features of the program are a revised attainable thrust estimation method to provide more accurate predictions for low Mach numbers, and a choice of three options for estimation of leading-edge separation vortex flow effects.

Comparison of program results with low speed experimental data for an arrow wing supersonic cruise configuration with leading-edge and trailing-edge flaps showed good agreement over most of the range of flap deflections. Other force data comparisons and an independent study of airfoil and wing pressure distributions indicated that wind-tunnel measurements of the aerodynamic performance of twisted and cambered wings and wings with leading-edge flaps can be very sensitive to Reynolds number effects.

17. Key Words (Suggested by Author(s)) Subsonic aerodynamics Numerical methods Leading-edge thrust Wing flaps Vortex lift Linearized theory	18. Distribution Statement FEDD Distribution Subject Category 01		
19. Security Classif. (of this report) Unclassified	20. Security Classif. (of this page) Unclassified	21. No. of Pages 72	22. Price

Available: NASA's Industrial Applications Centers